Materials for Renewable and Sustainable Energy
https://doi.org/10.1007/s40243-023-00254-3

ORIGINAL PAPER

The future of tire energy: a novel one-end cap structure for sustainable energy harvesting

Ibrahim Ali Al-Najati[1] · Abbas F. Jasim[2] · Keng Wai Chan[1] · Swee-Yong Pung[3]

Received: 29 June 2023 / Accepted: 28 December 2023

Abstract

Piezoelectric energy harvesting is gaining popularity as an eco-friendly solution to harvest energy from tire deformation for tire condition monitoring systems in vehicles. Traditional piezoelectric harvesters, such as cymbal and bridge structures, cannot be used inside tires due to their design limitations. The wider adoption of renewable energy sources into the energy system is increasing rapidly, reflecting a global attraction toward the utilization of sustainable power sources (Aljendy et al. in Int J Power Energy Convers 12(4): 314–337, 2021; Yesner et al. in Evaluation of a novel piezoelectric bridge transducer. In: 2017 Joint IEEE International Symposium on the Applications of Ferroelectric (ISAF)/International Workshop on Acoustic Transduction Materials and Devices (IWATMD)/Piezoresponse Force Microscopy (PFM). IEEE, 2017). The growing interest in capturing energy from tire deformation for Tire Pressure Monitoring Systems (TPMS) aligns with this trend, providing a promising and self-sustaining alternative to traditional battery-powered systems. This study presents a novel one-end cap tire strain piezoelectric energy harvester (TSPEH) that can be used efficiently and reliably inside a tire. The interaction between the tire and energy harvester was analyzed using a decoupled modeling approach, which showed that stress concentration occurred along the edge of the end cap. The TSPEH generated a maximum voltage of 768 V under 2 MPa of load, resulting in an energy output of 32.645 J/rev under 1 MPa. The computational findings of this study were consistent with previous experimental investigations, confirming the reliability of the numerical simulations. The results suggest that the one-end cap structure can be an effective energy harvester inside vehicle tires, providing a valuable solution for utilizing one-end cap structures in high-deformation environments such as vehicle tires.

Keywords TSPEH · Piezoelectric energy harvesting · Tire strain · Sustainable energy · Smart tire · TPMS

List of Symbols

TPMS	Tire pressure monitoring system
DECEH	Dual end cap energy harvesters
COMSOL	Computational Modeling Solution software
MFC	Microfiber composite
D_i	Electrical displacement
S_j	Mechanical strain
d_{ij}	Piezoelectric coefficient
$\sigma_j,\ T_j$	Mechanical stress
ε_{ii}	Permittivity
E_i	Electric field
e_{ij}	Piezoelectric coefficient
s_{ij}	Elastic compliance coefficient
c_{ij}	Elastic stiffness coefficient
PZT	Lead zirconate titanate
PVDF	Polyvinylidene fluoride
L_p	Total length of the piezoelectric harvester
t_p	Piezoelectric transducer thickness
t_e	Epoxy adhesive layer thickness
$A\ L_\mathrm{p}$	Adhered length of the piezoelectric harvester to the substrate using an epoxy layer
$E\ L_\mathrm{p}$	Effective length of the piezoelectric harvester that performs the tension and compression
L_pf	Piezo-element final stretched a total length
δ_p	Length change in the piezo-element
δ_s	Curvature changes in substrate base boundary

✉ Abbas F. Jasim
abbas.jasim@uomustansiriyah.edu.iq

[1] School of Mechanical Engineering, Universiti Sains Malaysia, Engineering Campus, 14300 Nibong Tebal, Penang, Malaysia

[2] Department of Highway and Transportation Engineering, Mustansiriyah University, Baghdad, Iraq

[3] School of Materials and Mineral Resources Engineering, Universiti Sains Malaysia, Engineering Campus, 14300 Nibong Tebal, Penang, Malaysia

Published online: 16 February 2024

hd	Height of the transducer allowable deformation limit
ts	Substrate thickness
hs	Substrate height
ws	Substrate width
A_i	Original corner position of a piezoelectric harvester
B_i	Final corner position of the stretched piezoelectric harvester
C_i	Center of structure rotation
M_i	TSPEH model number
θ	Angle of model rotation

Introduction

The development of sustainable materials for energy harvesting technologies is critical to meeting the growing global requirement for clean energy [3]. The tire pressure monitoring system (TPMS) is a wireless technology that keeps track of the air pressure in tires and notifies drivers of under-inflation or other problems in real time, with a growing interest in harnessing energy from tire deformation for this purpose [4]. By preventing tire failure due to improper pressure, TPMS can increase tire safety, fuel efficiency, and reduce tire wear [5]. The Firestone tire recall in the late 1990s, which was connected to more than 271 deaths and 800 injuries as a result of tire tread separation, served as one of the driving forces behind the development and widespread use of TPMS [6]. The TREAD Act, which was approved by the US Congress in 2000 as a response, made TPMS mandatory in all light motor vehicles sold after 2007 [7]. Later, several countries around the world adopted legislation requiring vehicle manufacturers to install TPMS in their tires [8]. TPMS is typically powered by batteries. However, these batteries can have a negative impact on the environment when they need to be replaced. Additionally, if the TPMS malfunctions due to low or dead batteries, it can result in dangerous tire damage. In most cases, it is not economical to replace all the TPMS when their batteries run low. As a result, piezoelectric energy harvesting has emerged as a promising and self-sustaining energy source for powering TPMS. This technology allows for the storage of energy in capacitors for later use [9, 10]. This makes tire-embedded piezoelectric energy harvesters a sustainable solution for powering TPMS. When mounting energy harvesters inside vehicle tires, there are two common energy sources: tire deformation and vibration. Of these two options, deformation energy is more viable than vibration energy. This is due to several limitations of tire vibrational transducers, including difficulty in matching frequencies, transducer location, and proof mass characteristics [11]. These limitations make them inadequate for multi-directional tire deflection [12, 13]. Additionally, the cantilever beam is difficult to stabilize when using the vibration scavenging method inside tire [12]. Furthermore, due to the vibration harvester's small size as compared to the host size, the resonance frequency cannot be matched [14]. In contrast, strain energy harvesting is a more convenient and efficient option [15]. Strain energy harvesting structures are usually more simple than vibrational ones. However, a high-flexible material must be used to harvest high tire strain. Different configurations of tire strain transducers have been fabricated, and the strain harvester assembly depends on the type of excitation applied, such as bending and pressing.

Overview: vehicle tire piezoelectric energy harvesting technologies

Vehicle tire wasted energy refers to the energy that is lost when a tire deforms during motion on the road. Piezoelectric energy harvesters can convert this wasted energy into usable electric energy. Researchers have attempted to transduce these energies by installing harvesters close to the tire–road interaction. The installation location of the harvester can be classified into two types: outside vehicle tire and inside vehicle tire harvesters. The characterization of each type depends on the host environment. For instance, if the harvester is installed outside the vehicle tire, which is usually inside the road pavement, it should be able to withstand high traffic stresses and climate changes. Additionally, if the harvester is installed inside the vehicle tire, it should be highly flexible, lightweight, and durable to withstand the harsh environment of the tire, such as high pressure and vibration. The literature has been classified according to the position of the energy harvester and the working principle relative to the vehicle tire. In addition, this classification helps to understand how the outside tire harvesters can be adapted for inside tire application with some design modifications.

Inside vehicle's tire strain energy harvesters

To ensure a stable and dependable power source for tire pressure monitoring systems (TPMS), piezoelectric energy harvesters can be installed inside the vehicle tire in proximity to the TPMS. This way, the wasted energy can be effectively utilized when required. The typical approach involves adhering a piezoelectric element directly onto the inner liner of the tire. However, despite the simple installation process, these harvesters are susceptible to punctures and cannot be replaced or maintained [16]. Three main common piezoelectric shapes used by researchers inside vehicle tire square, circular and rectangular.

Makki et al. [17] discovered that the deformation of at least 8% of the entire treadwall surface occurred during tire rotation while measuring contact patch deformation

at various speeds using 40 rows of circular PZT elements. PZT material was preferred due to factors such as power efficiency, flexibility after 540 million cycles, and cost. To prevent damage to the harvester, adhesive was applied to the centerline of PZT elements, reducing the deformability of the PZT benders and, consequently, the energy generated. The research found that power could be increased by increasing the inner tire treadwall surface area, tire rotational speed, and piezoelement deflection. The maximum power generated during the experiment was 2.3 W. These results show the highest energy output achievable from a piezoelectric energy harvester mounted in a vehicle tire.

In their study, Kubba et al. [18] evaluated the viability of utilizing a piezoelectric fiber composite transducer (PFC) to generate power for TPMS from rolling tire deformation. The harvester should be placed in the middle of the tire contact patch, according to the results of the Abaqus finite element simulation. After examining different tire speeds and various loading values, it was found that the load has a more pronounced effect on tire deformation than tire rolling speed. This implies that higher levels of harvested energy can be obtained from greater tire deformation. Hence, the vehicle load has a greater impact on the amount of harvested energy. The highest energy was obtained during traction and braking, with a value of 48.5 μJ/rev at a speed of 10 km/h, after considering the three tire rolling circumstances of free rolling, traction, and braking. Lee and Choi [19] demonstrated an interdigitated piezoelectric energy harvester integrated in an inner tire. Under 500 kgf load and 60 km/h, the study demonstrates that a piezoelectric energy harvester generates 380.2 μJ/rev. Nevertheless, the harvester could only scavenge a quarter of the tire available strain because of the inadequate adhesive flexibility. This issue could be addressed using a more flexible adhesive material while also considering other adhesive properties such as high lifecycle. Another source of energy loss was in electrical storage, which was estimated to be 90.1%. This was due to the leakage in the first and second capacitors. This can be avoided using high-quality capacitors and avoiding conditions with humidity and high temperatures.

A study presented by Aliniagerdroudbari et al. [20] involves modifying the upper end cap of the DECEH to have legs that can be adhered inside tire, securing the piezoelectric element in place and applying the necessary stress to harvest electrical energy for inside tire sensors. Aliniagerdroudbari et al. [20] introduced a transducer that is inspired from the Cymbal piezoelectric energy harvesters. The energy harvester consists of two flexible metal substrates, two supporting legs, and a piezoelectric material layer. The authors utilized COMSOL Multiphysics modeling to analyze the proposed harvester's performance. The results demonstrate that the harvester can conserve a significant portion of tire strain energy, thus generating an output electric energy and voltage of approximately 5 mW and 7 V, respectively, when subjected to a force of 500 kgf and a vehicle speed of 41 km/h. However, it should be noted that the tire analysis was not discussed in the study.

The limited number of researchers experimenting with piezoelectric energy harvesters mounted inside vehicle tires can be attributed to several difficulties. The complex and dynamic nature of the tire structure makes it challenging to accurately predict and model the strain and stress patterns within the tire, which can significantly impact the performance of the energy harvester. Additionally, the harsh environment inside the tire, characterized by high stresses, vibrations, and pressure, poses significant challenges in designing energy harvesting structures that can withstand these conditions while maintaining high harvesting efficiency. To address these challenges, a novel structure is required that can provide both durability and high harvesting efficiency in the high-strain environment of a tire. One promising approach is to implement an inspired structure from DECEH, which has several advantages over traditional piezoelectric harvesters, such as higher energy density, larger deformation and stress range.

Outside vehicle's tire stress energy harvesters

Dual end cap energy harvesters (DECEH) have gained significant attention as promising devices for harvesting high-stress energy by exploiting piezoelectric elements. In these devices, the external load applied to the energy harvester is transmitted to the piezoelectric material through the end caps, making the shape of the transducer a critical factor that affects the amount and distribution of stress transferred to the piezoelectric element. The DECEH structures include cymbal, bridge, arc, and arch configurations, with each configuration having a different deformation mode. The bridge structure undergoes bending deformation when subjected to an external force or vibration, while the cymbal structure undergoes both bending and twisting deformation due to the lateral expansion of the piezoelectric disk. The arch structure undergoes flexural deformation, whereas the arc structure undergoes axial deformation due to the compression or tension of the curved beam.

Few previous studies have attempted to incorporate DECEHs inside vehicle tires. However, the harsh environment within the tire has posed significant challenges. This is because most DECEHs are designed for low deformation and high stress, which are not suitable for high-deformation applications like vehicle tires. In addition, the operation of DECEHs differs from that of tire strain piezoelectric energy harvesters (TSPEHs). This is because DECEHs require a fixed end cap while the force or stress is applied to the other end cap. This cannot be applied inside vehicle tire, as it could compromise tire stiffness and safety. Instead, one of

the primary applications of DECEH structures is converting traffic loading wasted energy into usable electrical energy when embedded in asphalt pavement due to their ability to withstand high applied stresses. Additionally, DECEH targets both d_{33} and d_{31} piezoelectric coefficients, allowing for harvesting more electrical energy from the same external stress.

Several studies were carried out on investigating dual end cap energy harvesters (DECEH). In their study, Yao et al. [21] examined the efficiency of piezoelectric Bridge transducers for energy harvesting from asphalt pavement. The authors compared the performance of Arc and trapezoidal Bridge transducers under various frequencies and distributed loads, investigating their efficiency and storage electric energy under different conditions. The study found that the energy converting efficiency of Arc Bridge transducer was higher than that of trapezoidal Bridge transducer, and both types of transducers were able to operate under 0.4 MPa pressure in the pavement. The maximum voltage output measured from the arc Bridge transducer under 5 Hz half-sine loads and 0.4 MPa was 232 V, while for the trapezoidal Bridge transducer, it was only 106 V under the same conditions. These findings suggest that the arc Bridge transducer may be a more efficient option for energy harvesting from asphalt pavement. In the same manner, the arc bridge structure can be more suitable for inside tire application.

C. Li [22] conducted a study on the efficiency of piezoelectric transducers for energy harvesting from asphalt pavement. The study compared the performance of different types of piezoelectric transducers, such as Bridge, Cymbal, Moonie, Multilayer, Thunder, and Microfiber Composite (MFC) piezoelectric transducers. The results showed that the arc transducer generated a significantly higher voltage output compared to the rectangular transducer under the same load and normal working conditions. On average, the voltage generated by the Arc transducer was 63% higher than that generated by the rectangular transducer. For example, the arc transducer generated a voltage of 220 V under 0.45 MPa stress, while the rectangular transducer generated only 160 V under 0.7 MPa stress. However, the arc transducer was found to be more susceptible to damage under low stress of 0.5 MPa, while the rectangular transducer did not show any damage even under high stress of 0.7 MPa. These findings are significant because they suggest that the arc bridge piezoelectric transducer can produce higher voltage output, but its mechanical robustness should be carefully considered for practical applications. Further, the arc bridge can be installed inside tire after redesign the structure to be more suitable for inner tire environment.

In a study by Kim et al. [23], the effectiveness of a piezoelectric cymbal transducer was evaluated for generating electrical power from vibrations. This transducer consisted of a piezoelectric ceramic disk that was placed between two metal endcaps. The experiment involved applying a 70 N force within a frequency range of 10–200 Hz. The results indicated that the transducer generated approximately 100 mW of power at 200 Hz, with a 200 kΩ resistor in the circuit. The metal endcaps used in the transducer design not only increased the endurance of the ceramic but also amplified the stress to sustain high loads. However, the cymbal bridge transducer might not fit well inside tire compared to the arc bridge transducer. This is because on one hand, the cymbal structures usually have a flat or low curved shape that can affect tire flexibility. On the other hand, the arc bridge can be redesigned with matching its radius with tire radius for perfectly adhesion without influencing tire stiffness.

Yesner, Kuciej [24] developed a multi horizontal poled rectangular bridge transducer using a novel six-electrode piezoelectric material. The poling process was carried out at 80 °C with 2.15 kV/mm high voltage applied for 10 min, parallelizing the poling direction with the end caps' stresses direction applied to the piezoelectric element. The resulting output power of 2.1 mW was achieved using an 88 nF capacitor with 226.8 kg load at 5 Hz. Yesner, Safari [25] later reported that connecting 64 of these transducers in parallel generates 2.6 mW power under a 226.8 kg load with a 300 KΩ resistive load. One of the main structural failure causes reported was end caps de-bonding due to insufficient thickness of the epoxy layer after 350,000 load cycles. However, the rectangular bridge cannot be implemented inside vehicle tire due to end caps shape that cannot fit with tire curved rubber.

Jasim, Wang [26] enhanced the design of the multi-poled bridge transducer by studying the effect of geometrical parameters on the stresses applied to the piezoelectric element using COMSOL software. They found that steel end cap thickness and cavity height had more influence on the resulting stresses than geometrical parameters, which may be attributed to the nature of the bridge structure design where forces can be applied vertically. This is important because increasing the stress applied to the piezoelectric element leads to an increase in the resulting output energy. Since end caps' parameters has a more influence on harvester's performance compared to other factors, it is crucial to design an end cap fully compatible with tire inner liner. Hazeri and Mulligan [27] conducted an experiment to measure the voltage and power output of piezoelectric elements attached to the outer surface of tires under varying conditions of weight, air pressure, and speed. They discovered that the potential for harvesting energy from piezoelectric tires is the highest when the elements are connected in parallel circuits and when the tires experience higher compressive stress. The maximum harvested energy at maximum velocity was 0.035 μW. The amount of energy generated is directly proportional to the number of piezoelectric elements and the speed of the vehicle. They concluded that a vehicle could

generate up to 7.84 μW of energy per one complete rotation at 100 km/h using piezoelectric tires. However, the experiment cannot be applied on real vehicle tire for many reasons. First, the piezoelectric elements adhered to the outer surface of the tire which isolate the tire rubber from contacting road pavement. This can directly affect tire stability, braking, and controlling on roads. Secondly, the harvesters can easily crack due to the large amount of cyclic tire stress from the vehicle load. Not only that, due to tire rotation nature and centrifugal forces, the piezoelements could disassemble at increased tire speed. Lastly, it is not clear about how the harvested energy from outer surface of tire could be utilized, for example for powering inside tire-embedded sensors. To identify the most suitable configuration for piezoelectric harvesters excited by external stresses, a comprehensive analysis of the advantages and disadvantages of various piezoelectric harvester shapes has been presented in Table 1.

Research problem and study objectives

The use of piezoelectric energy harvesting inside vehicle tires presents a significant challenge due to the high-deformation and frequency environments present. Previous research has shown that the bridge and cymbal transducers, which require a force/stress from one side and a fixed other side, are not suitable for use inside vehicle tires. Furthermore, the use of such transducers inside tires can negatively impact tire flexibility and safety. As such, there is a need for a new structure that is specifically designed for use inside vehicle tires. In this study, a novel single substrate one-end cap transducer was implemented and analyzed under tire working conditions. The primary objective of this research is to optimize the design of this new structure by collecting tire data using Abaqus and applying it to the piezoelement and substrate structure using COMSOL software. This study aims to fill the existing research gap by addressing the need for a reliable and efficient energy transducer for use inside vehicle tires. The host environment should be thoroughly investigated to gain a deeper understanding of the energy harvester. As the primary objective of this study is to harvest wasted tire strain energy, it is imperative to model the car tire to identify its strain value and other factors that may impact the efficiency of energy transduction. The second objective of this study is to determine the optimal location for the piezoelectric harvester inside the vehicle tire by identifying the point of maximum strain/stress within the tire. The transducer's size and dimensions can then be designed based on the tire analysis. The third objective is to demonstrate the simulation process for the piezoelectric harvester and the supporting Aluminium substrate using COMSOL Multiphysics solver. This step is crucial in determining the optimum dimensions for maximum energy harvesting efficiency. In COMSOL software, various scenarios can be considered simultaneously in the model, such as the inclusion of an electrical circuit setup and cyclic changeable load. The study objectives are presented in Fig. 1, which outlines the study's flowchart.

Table 1 Different configurations of DECEH

Configuration	Advantages	Limitations
Cymbal	Difficult geometry fabrication Exploits both piezoelectric coefficients d_{31} and d_{33} [28] Enlarges the stress applied to the piezoelement	Only suitable for situations requiring high-magnitude vibration sources [29] The energy produced by a single piezoelectric harvester is comparatively small [30]
Traditional Bridge	Utilizes the d_{33} piezoelectric coefficient for doubling energy output [28] Enlarge stress applied to the piezoelement	Not suitable for inside vehicle tire energy harvesters More expensive because it requires a larger piezoelectric material element
Arc	Can generate high-power output with low deformation input Easy to fabricate compared to other structures	Requires a precise fabrication and assembly due to its curved end caps Require a larger piezoelectric element compared to arch
Arch	Can generate high-power output with low-deformation input Suitable for applications with limited available space	Requires a precise fabrication and assembly due to its curved end caps Limited to low-amplitude vibrations
Multi-poled bridge	Produces high energy Utilizes the d_{33} piezoelectric coefficient for doubling energy output	It has a high fabrication cost Not suitable for inside vehicle tire energy harvesters
This study new one-end cap structure	Suitable for inner tire usage due its high flexibility Able to maintain a large stress input Exploits both piezoelectric coefficients d_{31} and d_{33}	Maintains less applied load than the bridge design due to using a single base cap instead of double caps

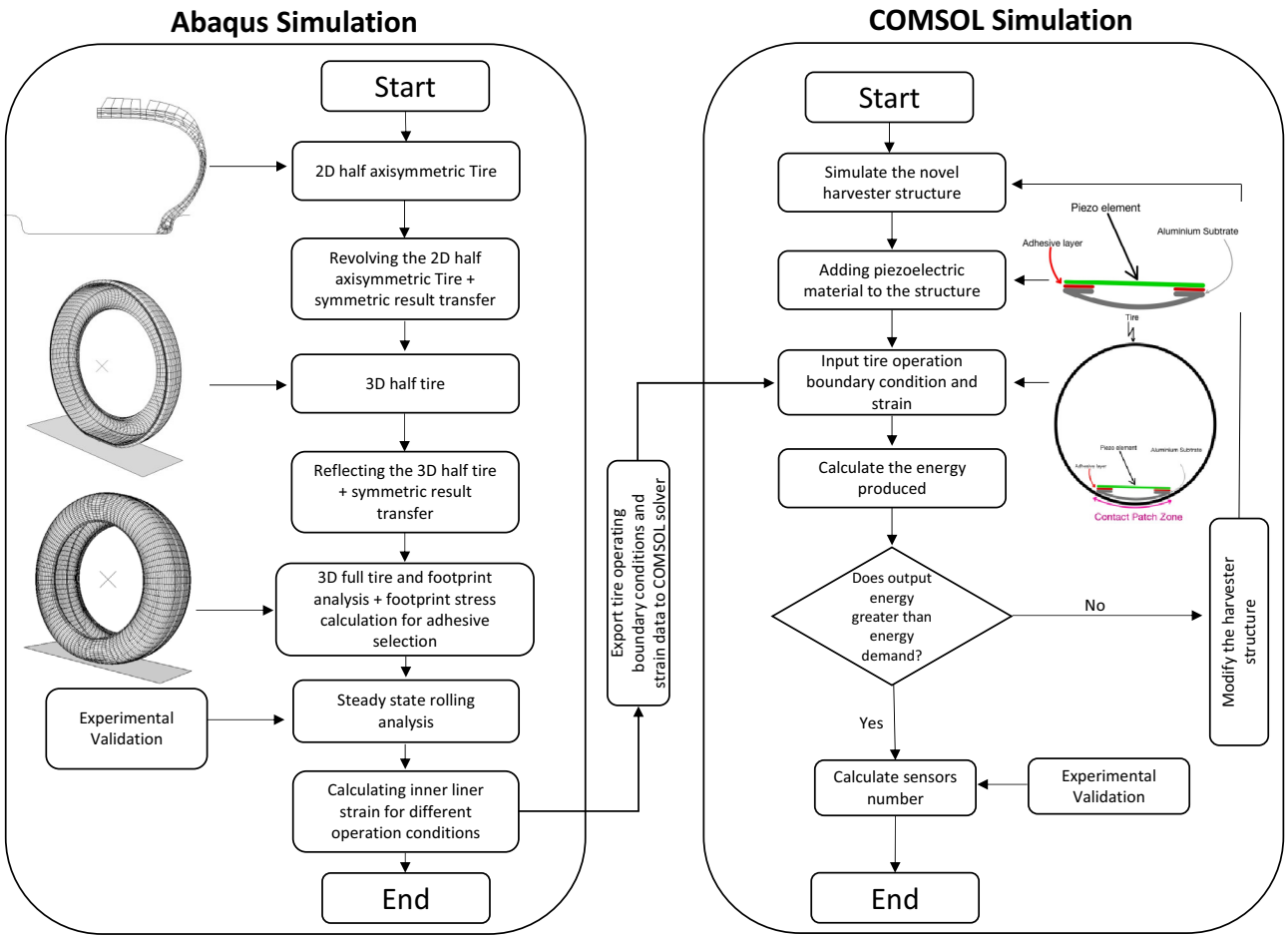

Fig. 1 Study flowchart

Theoretical background of piezoelectric effect

The working principle of piezoelectric materials can be described as follows: when the material bends due to tire deformation, a charge is generated [31]. The piezoelectric energy harvesting mechanism is illustrated in Fig. 2 and consists of three main parts: the wasted energy, the harvester structure, and the final electrical load [32]. To convert the wasted energy into a proper load, it is necessary to choose the appropriate piezoelectric material [33]. The polarization of piezoelectric materials is usually randomly oriented [34], so a polarization process is required to permanently align the crystal dipoles by applying a high electrical field to the material. This process is depicted in Fig. 3.

Figure 4 shows the most common operating modes of piezoelectric materials. The d_{31} piezoelectric mode is commonly used in harvesting tire strain applications because the tire stress applied to the piezoelement is usually perpendicular to the polling direction of the piezoelement. However, targeting the d_{31} mode only, usually produces less energy than considering both d_{31} and d_{33} modes. To target the d_33 mode of the piezoelement, a polarization process should be applied to the piezoelement to align the polling direction with the deformation/force direction. Additionally, using the new substrate structure will convert the vertical tire inner liner stress to horizontal stress along the X-axis at the piezoelectric substrate contact region. The d_{15} shear mode is not related to this study main topic.

Piezoelectric materials are smart materials that can work in two modes, the direct and reverse actuator modes, when an electric field or load is applied to the material [35]. The direct mode, as shown in Fig. 5a, occurs when the piezoelectric material is deformed due to an external force or deformation. On the other hand, the same piezoelectric material can work as an actuator, as shown in Fig. 5b, when an external electric field is applied to the material.

The direct and inverse piezoelectric modes can be described as mathematical models presented below in Eqs. (1) and (2) [36] where the linear elastic material

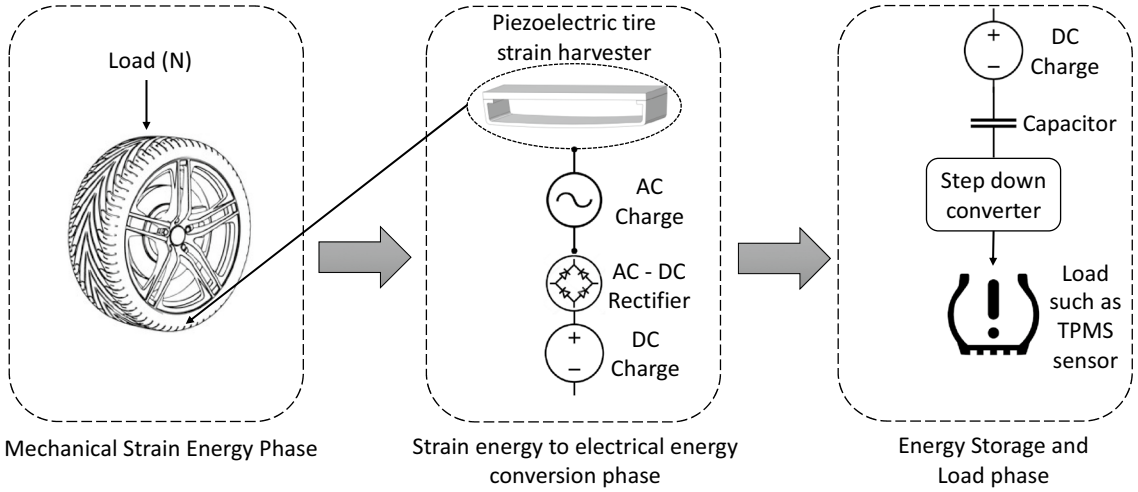

Fig. 2 Energy harvesting block diagram

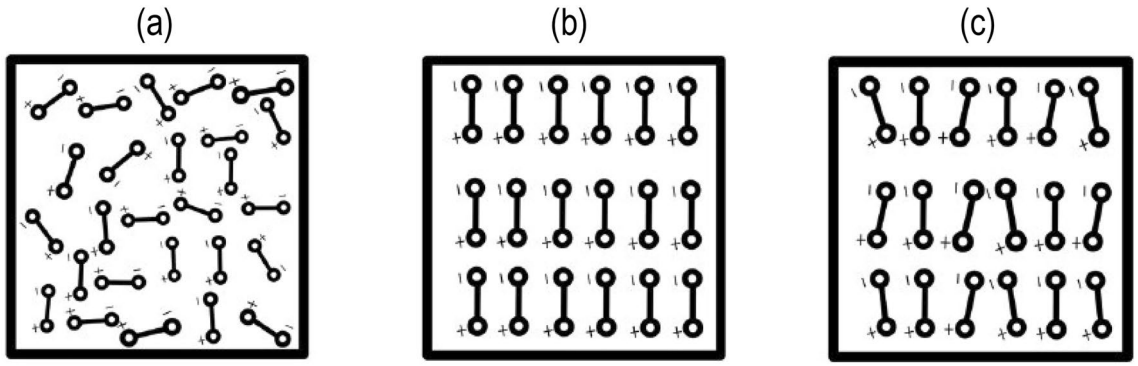

Fig. 3 Crystals orientation **a** before **b** during and **c** after polarization process

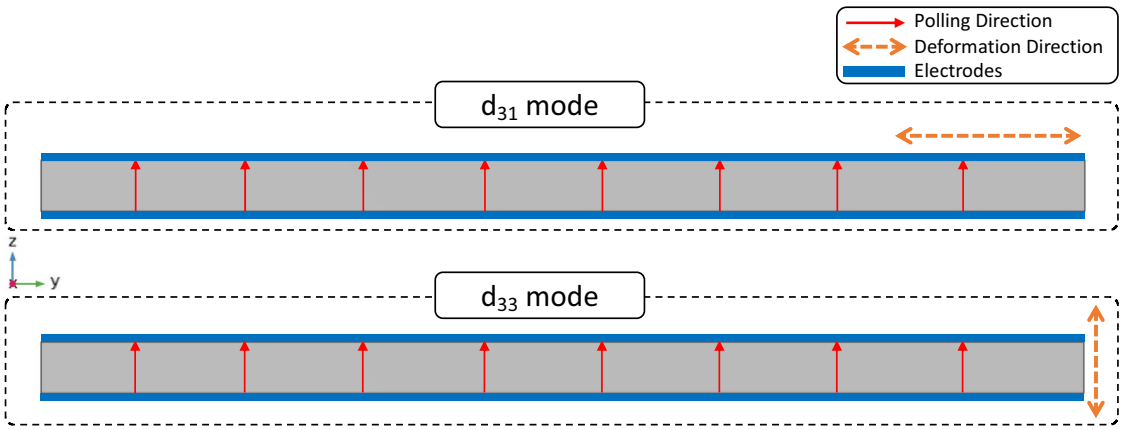

Fig. 4 Configuration of d_{31} and d_{33} piezoelectric modes

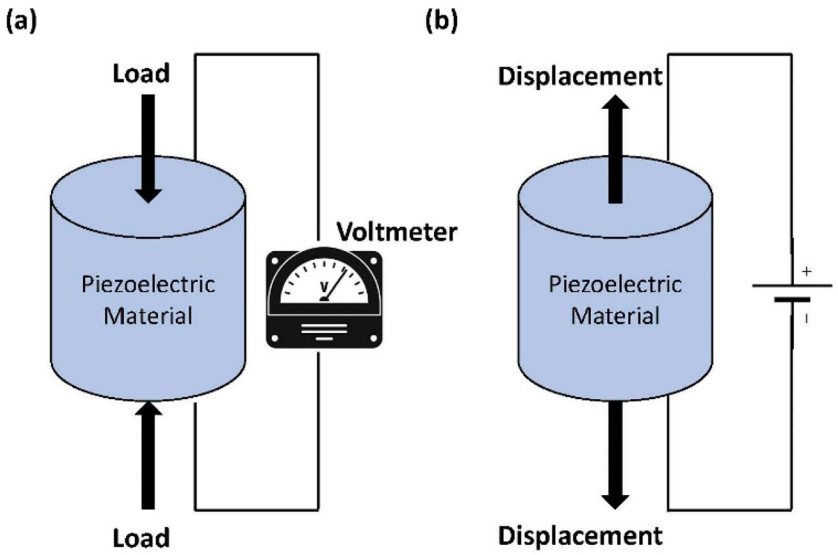

Fig. 5 Direct and reverse effect of piezoelectric materials

characteristics of piezoelectric materials can be stated as follows:

$$D_i = d_{ij}T_j + \varepsilon_{ii}^{T}E_i, \tag{1}$$

$$S_j = s_{ij}^{E}T_j + d_{ij}E_i. \tag{2}$$

The above-coupled Eqs. 1 and 2 represent the constitutive equations in strain-charge form. Additionally, same questions can be written in a stress-charge coupled form as indicated in Eqs. (3) and (4):

$$D_i = e_{ij}S_j + \varepsilon_{ii}^{S}E_i, \tag{3}$$

$$T_j = c_{ij}^{E}S_j - e_{ij}E_i. \tag{4}$$

Equations (3) and (4) can be written in a matrix form as follows:

$$\begin{bmatrix} D_1 \\ D_2 \\ D_3 \end{bmatrix} = \begin{bmatrix} e_{11} & e_{12} & e_{13} & e_{14} & e_{15} & e_{16} \\ e_{21} & e_{22} & e_{23} & e_{24} & e_{25} & e_{26} \\ e_{31} & e_{32} & e_{33} & e_{34} & e_{35} & e_{36} \end{bmatrix} \begin{bmatrix} S_1 \\ S_2 \\ S_3 \\ S_4 \\ S_5 \\ S_6 \end{bmatrix} + \begin{bmatrix} \varepsilon_{11} & \varepsilon_{12} & \varepsilon_{13} \\ \varepsilon_{21} & \varepsilon_{22} & \varepsilon_{23} \\ \varepsilon_{31} & \varepsilon_{32} & \varepsilon_{33} \end{bmatrix} \begin{bmatrix} E_1 \\ E_2 \\ E_3 \end{bmatrix} \tag{5}$$

$$\begin{bmatrix} T_1 \\ T_2 \\ T_3 \\ T_4 \\ T_5 \\ T_6 \end{bmatrix} = \begin{bmatrix} c_{11}^{E} & c_{12}^{E} & c_{13}^{E} & c_{14}^{E} & c_{15}^{E} & c_{16}^{E} \\ c_{21}^{E} & c_{22}^{E} & c_{23}^{E} & c_{24}^{E} & c_{25}^{E} & c_{26}^{E} \\ c_{31}^{E} & c_{32}^{E} & c_{33}^{E} & c_{34}^{E} & c_{35}^{E} & c_{36}^{E} \\ c_{41}^{E} & c_{42}^{E} & c_{43}^{E} & c_{44}^{E} & c_{45}^{E} & c_{46}^{E} \\ c_{51}^{E} & c_{52}^{E} & c_{43}^{E} & c_{54}^{E} & c_{55}^{E} & c_{56}^{E} \\ c_{61}^{E} & c_{62}^{E} & c_{63}^{E} & c_{64}^{E} & c_{65}^{E} & c_{66}^{E} \end{bmatrix} \begin{bmatrix} S_1 \\ S_2 \\ S_3 \\ S_4 \\ S_5 \\ S_6 \end{bmatrix} - \begin{bmatrix} e_{11} & e_{21} & e_{31} \\ e_{12} & e_{22} & e_{32} \\ e_{13} & e_{23} & e_{33} \\ e_{14} & e_{24} & e_{34} \\ e_{15} & e_{25} & e_{35} \\ e_{16} & e_{26} & e_{36} \end{bmatrix} \begin{bmatrix} E_1 \\ E_2 \\ E_3 \end{bmatrix} \tag{6}$$

Finite element model development

Tire modelling

The host environment (in this case vehicle tire) should be thoroughly investigated to gain a deeper understanding of the energy harvester working environment and available wasted energy. As the primary objective of this study is to harvest wasted tire strain energy, it is imperative to model the car tire to identify its strain value and other factors that may impact the efficiency of energy transduction. Secondly, it is essential to determine the optimal location for the piezoelectric harvester inside the vehicle tire by identifying the point of maximum strain/stress within the tire. The transducer's size and dimensions can then be designed based on the tire analysis.

The tire was modelled as an axisymmetric model instead of a full 3D model because a full tire 3D model requires 50–100 times as many elements as an axisymmetric model, making it impossible to run on normal computers (Abaqus documents). The tire cross section was built using five components: carcass, belts, bead, plies, and rim, which can be assembled to form a 175/65 R14 tire size. Figure 6 illustrates the five primary tire parts.

Using the parts editor in the software and following Abaqus tutorials, three main parts were created: tire carcass, rim, and tire plies. Skins and surfaces were created to apply properties, loads, boundary conditions, and interactions. Two main surfaces were applied: tire pressure and rim–tire contact interaction. The assigned inflation pressure was 200 kPa, which was applied to the inner tire liner. The rim was assigned as a rigid body. Figure 7 indicates the tire modeling steps.

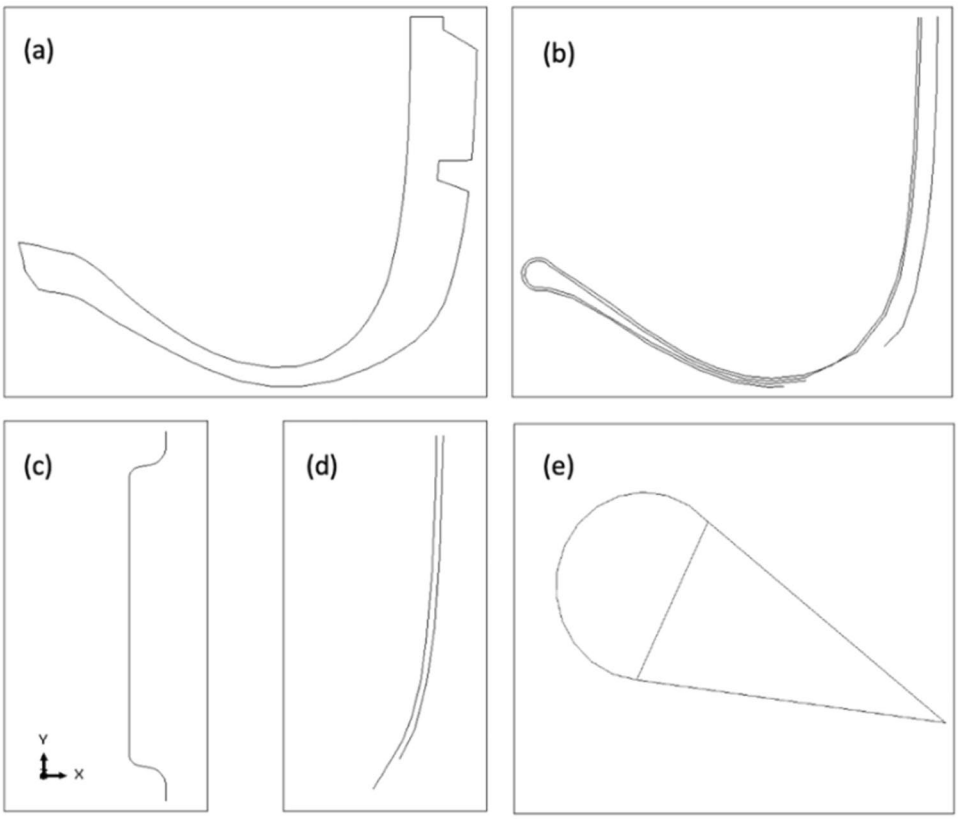

Fig. 6 Tire components: **a** carcass **b** plies **c** rim **d** belts **e** bead

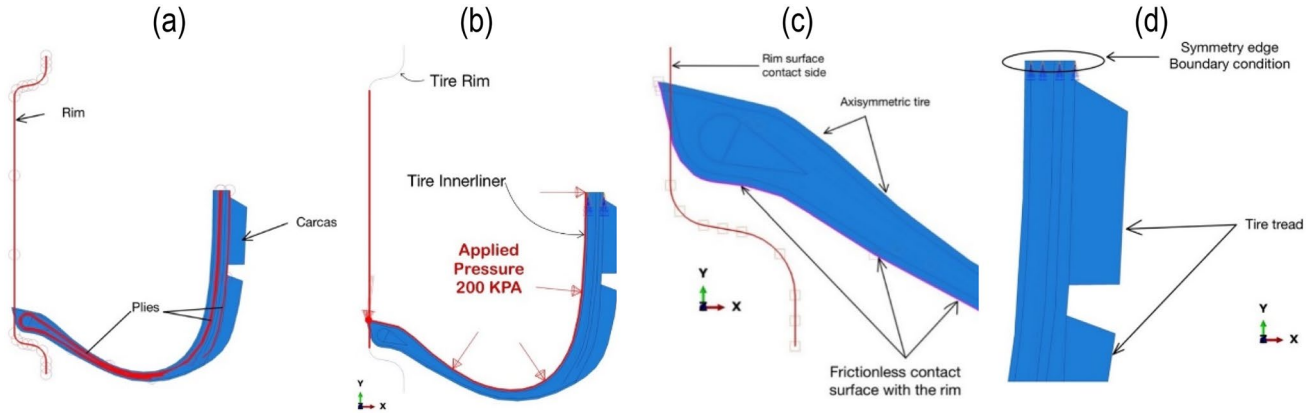

Fig. 7 **a** axisymmetric tire parts, **b** applied pressure to tire inner liner **c** tire–rim interaction, **d** the symmetry edge boundary condition location

The tire's material behavior was set to be elastic and hyper-elastic. Most of the material properties were set automatically from the material library in the software. However, some properties were entered manually, and for hyper-elastic materials, a Neo-Hookean strain energy potential was used. Table 2 displays the elastic and hyper-elastic tire material properties used in the Abaqus solver.

Before running the tire analysis, two steps were considered: mounting and pressurization. In the mounting step, the rim rigid body displacement was applied to simulate the rim mounting interaction with frictionless interaction, and the mechanical tangential behavior was set as the contact property. Additionally, the nonlinear effect of large displacements was turned on, and the automatic shrink-fit technique was used to gradually remove overclosure at the tire–rim interface. The incrementation setting was set to automatic with a maximum number of increments of 100, and the initial increment size was 0.1 with a minimum value of (1×10^{-5}) and a maximum value of one. For the

Table 2 Elastic and hyper-elastic tire components' properties

Part name	Mechanical behaviour	Young's modulus (MPa)	Poisson's ratio	Mass density (kg/m^3)	Material density (kg/m^3)	C10	D1
Rebar (steel)	Elastic	2.07×10^5	0.3	7.5×10^{-9}	–	–	–
Apex	Hyper-elastic	–	–	–	1.1×10^{-9}	6.0	0.003
Rubber	=	–	–	–	1.1×10^{-9}	0.6	0.03
Inner liner	=	–	–	–	1.1×10^{-9}	1.5	0.010
Side Wall Compound	=	–	–	–	1.1×10^{-9}	1.5	0.010
Tread	=	–	–	–	1.1×10^{-9}	0.5	0.040

pressurization step, the pressure load was applied. A step restart request was set to 999 for this step.

Meshing generation was established after partitioning the carcass geometry into several regions. This minimized the meshing process time and provided a finer mesh near the tire–rim contact, belts end region, and groove region of the tread. A quadrilateral axisymmetric element shape was assigned to most regions of the model with the sweep technique applied. Furthermore, a triangular axisymmetric element shape with a free technique was assigned to a small triangle region in the model. Two element types (fully integrated, linear with twist) were assigned to the carcass region, namely CGAX3 and CGAX4 (named as in Abaqus software). Then, an MGAX1 membrane element with a twist appointed to the belts and plies. To verify mesh quality, a mesh analysis check was performed. This is because Abaqus may terminate the analysis if any poor-quality mesh is found. After that, the job was submitted, and the solution was visualized as discussed in the results part.

A half 3D tire can be generated by revolving the axisymmetric 2D half tire, as shown in Fig. 8a. It is important to mention that all model setup and solution were transferred to the revolved nodes and elements, such as contact, pressure, and material definition. Furthermore, a road is also modeled as a rigid surface separated from the tire tread by a small distance. A vertical load of 1650 N was applied to the tire (half of the total force = 3300 N). A full 3D tire was generated by reflecting the half symmetric 3D tire. Simultaneously, the symmetric results were transferred to the second half of the reflected tire. The full 3D tire is shown in Fig. 8b.

The steady-state tire rolling was assumed to be traveling on a straight line. Additionally, the angular velocity was equal to ground velocity (no traction or braking). Braking occurs when angular velocity decreases while traction caused by increasing angular velocity. The following Table 3 shows the main input parameters and the boundary conditions for the tire simulation using Abaqus software.

TSPEH model design

In this study, a novel substrate structure was developed. The new TSPEH structure imply a one-end cap to support the piezoelectric material to withstand high tire strain. Additionally, for maximizing efficiency, the new TSPEH pursuing the d_{33} charge constant and d_{31} charge constant for the piezoelectric material. Figure 9a shows the proposed structure, which features a curved substrate base designed to represent the contact region with the inner tire surface. The radius of curvature of the substrate base is equivalent to the vehicle tire radius, and the harvester length is limited to 50 mm to

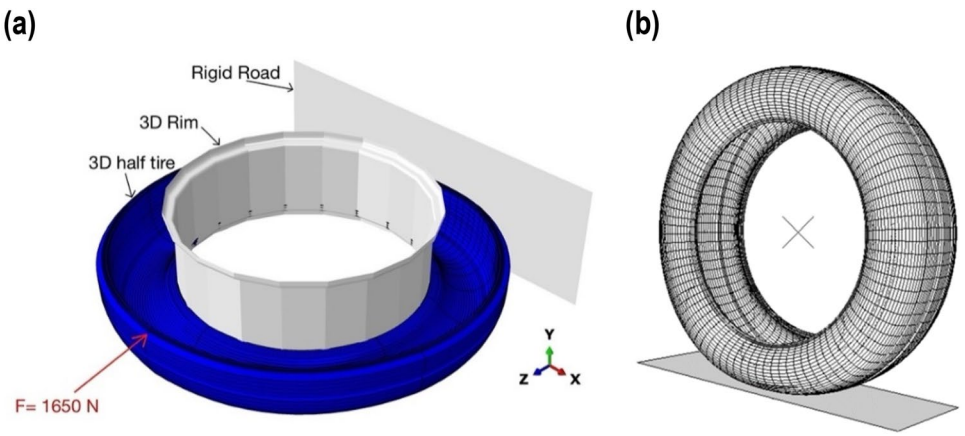

Fig. 8 **a** symmetric 3D tire generated in Abaqus, **b** full 3D tire with the contact surface

Table 3 Abaqus boundary conditions of 175/65 R14 Tire Analysis Steps

No	Step	Description	Value
1	2D half axisymmetric tire Generation Step	Symmetry edge boundary condition	2D half axisymmetric upper edge
2	Mounting Step	Rigid body	Tire rim
		Rim–tire interface Contact interaction	Frictionless contact/mechanical tangential behavior
		Rim–tire interface Large displacements	Nonlinear effect of large displacements
		Rim–tire interface Shrink-fit Technique	Gradual removal of overclosure
		Incrementation	Automatic with max. increments of 100
		Increment Size	Initial increment size 0.1, minimum value of (1×10^{-5}), maximum value of 1
3	Pressurization Step	Tire Inner liner Inflation pressure	200 kPa
4	Meshing step	A quadrilateral axisymmetric element shape was assigned with the sweep technique applied	Applied to most regions of the model
		A triangular axisymmetric element shape with a free technique was	Assigned to a small triangle region (on the left side of rim region) in the tire model
		Two element types of CGAX3 fully integrated and CGAX4 linear with twist	assigned to the carcass region
		MGAX1 membrane element with a twist	Appointed to the belts and plies
		Mesh analysis check	Applied to the full geometry
5	Half 3D Tire Generation Step	Revolving the axisymmetric 2D half tire	Applied to the full geometry
6	Road Generation step	Modeled as a rigid surface	Road that separated from the tire tread
7	Vertical load step	A vertical load of 1650 N (half of the total force = 3300 N)	Applied to the half 3D tire
8	Full 3D Tire Generation Step	Reflecting the half symmetric 3D tire	Applied to the half 3D tire
9	Steady-state full 3D tire rolling	Friction coefficient	0.5
		Ground velocity	80 km/h
		Angular velocity	%1.%2 s

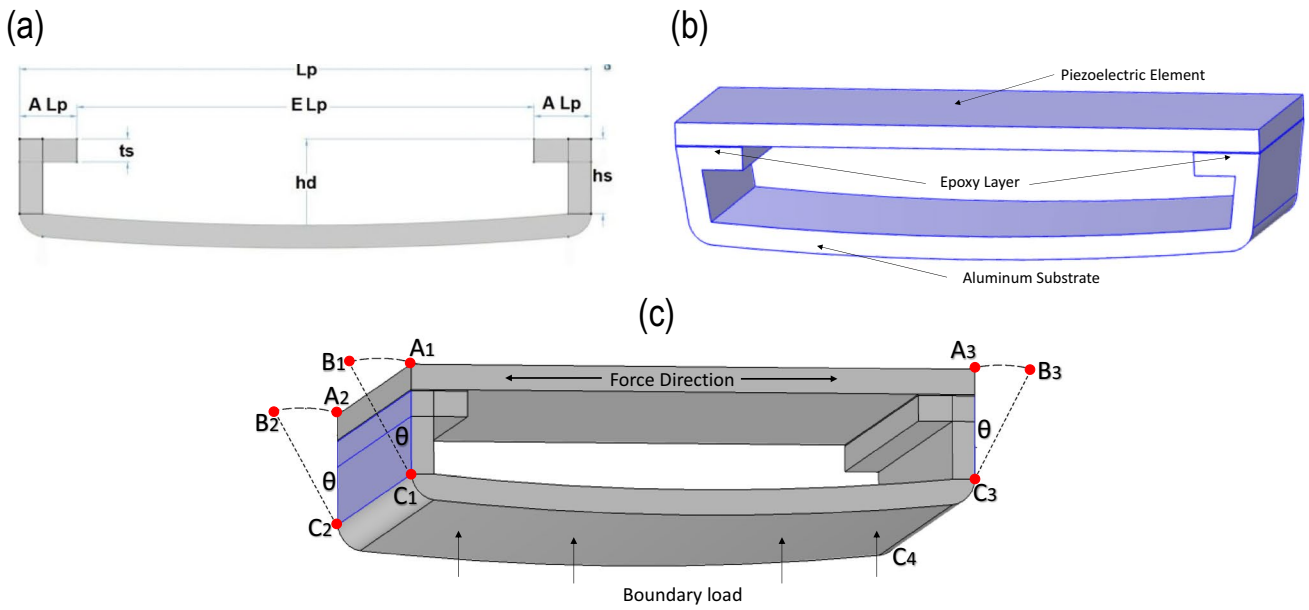

Fig. 9 The proposed model structure (M_i) for **a** new substrate **b** piezoelectric element adhered to the substrate **c** transducer movement mechanism before piezo-deformation

ensure that the maximum stress occurs inside the tire contact region.

The piezoelectric element is adhered to the Aluminum substrate using a filled epoxy resin (X238) with an initial thickness of 0.1 mm, as shown in Fig. 9b. To achieve a higher energy harvesting efficiency, the piezoelectric element is deformed due to a new substrate moving mechanism, represented in Fig. 9c. The rotational movement of the substrate supporting arms causes the piezoelectric element to follow an arc pathway instead of a linear deformation, resulting in a slight bending of the piezoelectric element. This bending enables energy harvesting in d31 mode in addition to the d33 mode. However, the bending of the piezoelectric element must not cause failure in the transducer structure and should remain below the yield point.

The piezoelectric transducer is adhered to the Aluminum substrate using an epoxy layer, and this region is represented in Fig. 9a as A_L_{p}. Hypothetically, the adhered region of the piezoelectric element will not produce energy since it behaves as a rigid body. Therefore, the only region that deforms horizontally along the X-axis is the effective piezoelement length (E_L_{p}), as shown in Fig. 9a. The total length of the piezoelectric element at a static condition can be represented by the following equation:

$$L_{\mathrm{p}} = EL_{\mathrm{P}} + 2AL_{\mathrm{p}}. \tag{7}$$

Since the adhered region of the piezoelectric element is assumed to be constant it will be presented as a constant value (α) in the above equation as follows:

$$L_p = EL_P + \alpha. \tag{8}$$

A rotational movement occurs for substrate sidewalls that move on an arc (A_i–B_i) pathway. As a result, the piezoelement bends slightly. The arc pathway is shown in Fig. 9c, where Ai represents the initial piezoelement coordinates before applying the boundary load, while Bi is the final location of the substrate side wall after applying the boundary stress. The center of substrate sidewall rotation is represented by point Ci.

The deformation of the piezoelectric element is assumed to be uniform and symmetric from both ends. The proposed increase in the piezoelement before deformation is represented in Fig. 10a. For mathematical representation only, the increase in piezoelectric material represented in the figure at both element ends. This is because in reality the deformation occurs uniformly along the piezoelement and not in one specific location.

The circular rotation of the radius represents the sidewall of the substrate, as shown in Fig. 10b. Figure 10c represents the transducer structure after applying the stress that causes an elastic deformation to the aluminum substrate and the piezoelectric element harvester. It can be seen that the piezoelement and the substrate was curved due to sidewall rotation. It is crucial to mention that arc length (A_{i}–B_i) from both sides ($2\delta_{\mathrm{p}}$) should be less than the maximum allowable deformation for the piezoelement.

When the piezoelement stretched from point A_i to point B_i, the increase in piezo-length can be calculated from arc $_{(}A_i$–$B_{i)}$ length as in the following equation:

$$\delta p = r\theta. \tag{9}$$

The circular rotation radius represents the sidewall of the substrate, as shown in Fig. 10b that can be calculated from the following equation:

$$r = h_{\mathrm{s}} + t_{\mathrm{e}} + t_{\mathrm{p}}. \tag{10}$$

The final extended piezoelement can be calculated as:

$$L_{\mathrm{pf}} = L_{\mathrm{p}} + 2\delta_{\mathrm{p}}. \tag{11}$$

From the above equations, the final length of the piezoelement can be represented as follows:

$$L_{\mathrm{pf}} = EL_{\mathrm{P}} + \alpha + 2\left(h_{\mathrm{s}} + t_{\mathrm{e}} + t_{\mathrm{p}}\right). \tag{12}$$

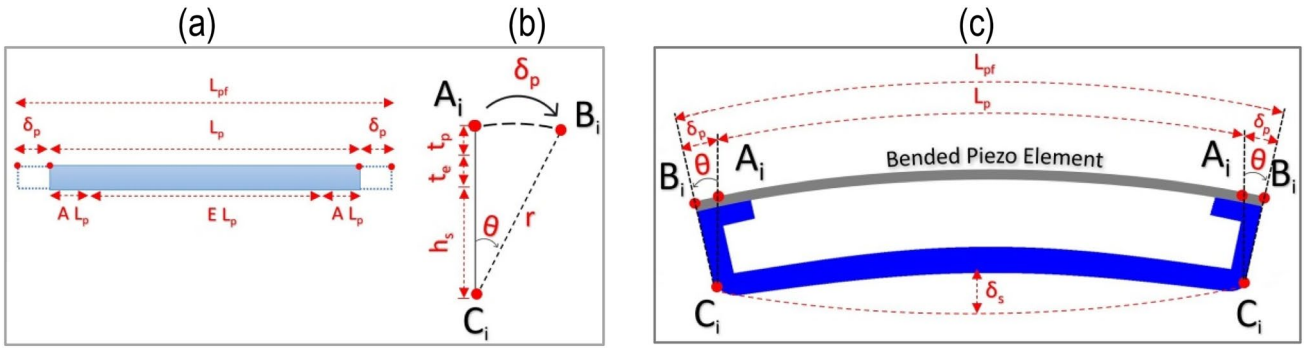

Fig. 10 Movement analysis for **a** piezoelement before bending **b** arc pathway **c** piezoelement and new substrate structure after bending

Mesh sensitivity analysis

Finer mesh provides more accurate results. However, a very fine mesh might be computationally expensive. A balance between result accuracy and computational resources must be taken into consideration. During the analysis, it was found that stress is concentrated at the corners of the aluminum harvester substrate. A mesh sensitivity analysis was conducted for von Mises stresses.

Figure 11a shows a clear relationship between different element sizes and the related von Mises stresses determined by mesh sensitivity analysis. It is noticeable that the shown von Mises stresses generally follow the expected pattern, exhibiting a predicted rise in stress as the element size reduces. Further, when the element size reduces (mesh becomes finer), the error decreases. However, the error become constant beyond 0.35 mm, suggesting that further mesh refinement does not notably improve the results accuracy. Therefore, in order to balance results accuracy and computational resources, an element size of 0.35 mm was fixed during all numerical analysis. Figure 11b shows the final meshed structure after refining the critical corners.

Transducer material

Various materials have been developed as a piezoelectric tire strain harvesting material; however, each piezoelectric material has its own drawbacks. For example, ceramic lead zirconate titanate PZT-4 and PZT-5 are widely used in tire-stain piezoelectric harvesters [37]. PZT materials have many advantages such as a high mechanical coupling factor [38], higher piezoelectric charge constant [39], and high operating temperature [40]. The fabrication process of pure PZT material is simple and inexpensive [41]. However, PZT ceramic material has some drawbacks such as lack of flexibility that reduce its lifespan and cause mechanical depoling due to high tire strain inputs [42]. Similarly, Polyvinylidene fluoride material (PVDF) offers a higher flexibility than PZT which means more compatibility to tire high-strain environment [14]. This is because PVDF is a flexible polymer material with piezoelectrical properties contrasting to PZT, a ceramic material. However, PVDF materials have inadequate thermal properties for use in automotive tires [31]. One of the fundamental aspects of piezoelectric operating temperature is the curing temperature, the temperature where the piezoelectric material loses its piezoelectric effect [43]. It has been reported that the PVDF curing temperature is in the range of 150–175 °C [44, 45]. While PZT material performance decreases slightly at a temperature range 150–250 where the PZT curing temperature is 250 °C [46]. PVDF also performs poorly in charge constant by around a third compared to PZT [40]. Because of the efficiency of the piezoelectric energy harvesters varies depending on the material properties, a comparison between PZT and PVDF materials was established in terms of the favorable properties as indicated in the Table 4 below. In this study, the PZT material was selected. This is because the only drawback of PZT is the low flexibility that can be enhanced using an aluminium substrate.

After generally considering the PZT material as the energy harvester material, the specific material type of PZT should be identified. One of the known transducer's material selection criteria is by Kim and Priya [23, 53] approach. They found that the most efficient piezoelectric material can be determined with maximum value of multiplying piezoelectric charge constant and piezoelectric voltage constant. This is because higher charge constant and higher voltage constant means greater potential energy. In other words, the highest electrical energy material has a highest ($g_{33}.d_{33}$) value. The 3–3 mode was selected for choosing the most efficient material suitable for this study application. The following Table 5 shows the important piezoelectrical material parameters that chosen for this study application based on the above selection criteria.

According to Table 5 above, PZT-5X was selected in this study as primary harvester material. This is because it has the maximum ($g_{33}.d_{33}$) value which leads to a highest electrical energy harvesting compared to other PZT types.

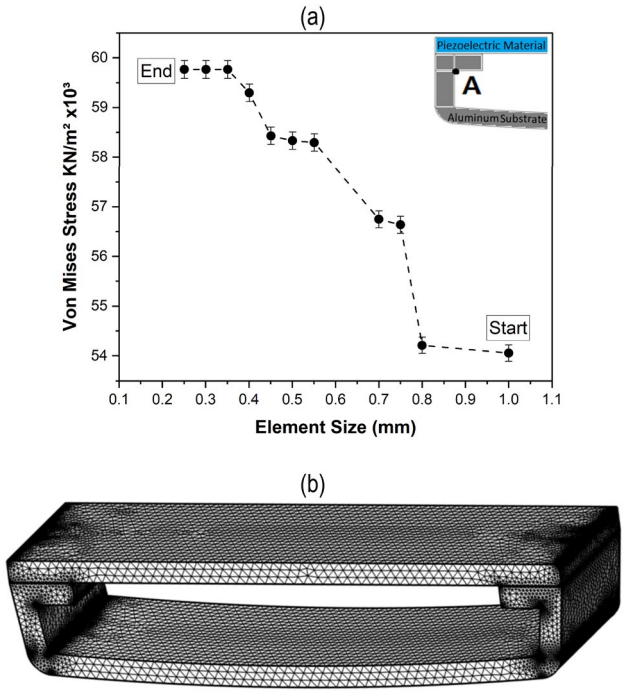

Fig. 11 Mesh sensitivity analysis results at point **a** for von Mises stress; **b** final meshed model

Table 4 Comparing favorable parameters for PVDF and PZT materials

Properties	Units	PZT	PVDF
Piezoelectric-charge constant	10^{-12} C/N	110 [47]	33 [47]
Flexibility	–	Low (–) [48]	Excellent (+) [19]
Service lifespan	year	Poor (–)	Good (+)
Service temperature	°C	Up to 250 (+) [46]	150–175 (–) [44, 45]
Output power density	mW m^{-2}	High (+) [49]	Low (–) [50]
Cost	$/cm	0.5 (+) (Circular shape area 78.5 cm^2) [51]	2 (–) (Rectangular sheet area 7400 cm^2) [52]

(+) favorable (–) unfavorable

Table 5 Important parameters for different PZT materials [54]

Material	d_{33} (P C/N)	g_{33} ($\times 10^{-3}$ Vm/N)	$d_{33}.g_{33}$ ($\times 10^{-15}$ Vm/N)
PZT-4	289	26.1	7542.9
PZT-5H	593	19.7	11,682.1
PZT-5X	750	19	14,250.0
PZT-7A	153	36	5,508.0
PZT-8	225	25.4	5,715.0

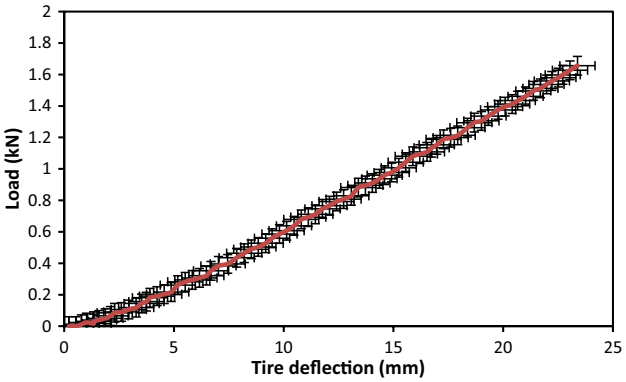

Fig. 12 Force displacement curve for 3d half static tire analysis

Results and discussion

Tire strain analysis

The results were accomplished for a stationary deformed tire and a steady-state rolling tire. The focus was on tire deformation and the developed tire strain. Additionally, the contact region was analyzed to find the suitable dimensions for the TSPEH structure. The maximum displacement at tire–road contact patch was 23.2 mm when a vertical force was applied of 1650 N (half of the total load of 3300 N). The strain predicted in this step is for a static tire (no angular velocity or linear velocity were applied). The behavior of the displacement change related to applied force was approximately linear. Figure 12 below indicates the force–displacement curve.

The displacement curve for a steady state rolling tire was predicted using the Abaqus program. The calculation was performed at a specific point/node that traverses the center of the tire contact region along the entire inner tire circumference. The maximum strain was found to occur at the center of the tension zone, which spans from 160° to 240°. The maximum displacement recorded during rolling was 16.711 mm and occurred at the center of the contact patch. To facilitate analysis, the tire was divided into 360 sections, with the first section located at the top of the tire (at 0°) and the center of the contact region located at 180°, where the maximum displacement is observed.

Figure 13 illustrates the deformation of a tire, which is divided into three zones based on the magnitude of the displacement. The two lowest deformation regions are compression zones, denoted as zone one and zone three in Fig. 13), with a displacement value of approximately -5 mm. The midrange displacement occurs at region 5, where the deformation gradually increases as the tire approaches the rigid surface and decreases gradually as the tire moves away from the surface, resulting in a tensioned zone. The maximum tire deformation occurs at the center of the tire–road interaction region, which is represented as region 4 in the graph, with a displacement value of 16.711 mm.

At the point of contact between the tire and the road, the maximum strain occurs. To analyze the harvester, it is important to determine the maximum host available dimensions, which indicates the maximum size limit of the harvester structure. The key point is to find the maximum contact area where the maximum strain occurs. Figure 14 illustrates the maximum host dimensions that produce the maximum vertical tire strain at the inner liner.

Figure 14a depicts the amount of tire strain in the -Zdirection at loading and unloading regions. The loading region exhibits a maximum strain of 16.711 mm in red color,

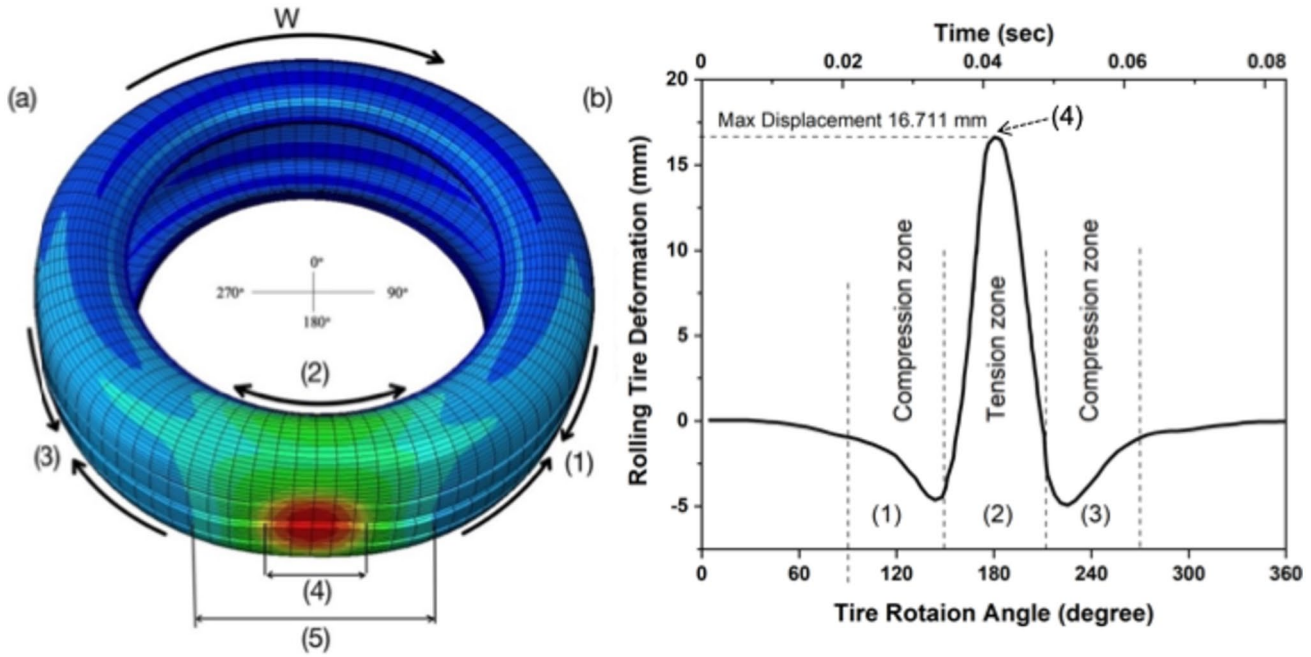

Fig. 13 **a** Deflection distribution at the contact patch region for a rolling tire on a rigid surface **b** displacement magnitude with respect to rotation angle

located in the middle of the tire–pavement interaction or tire footprint. The unloading zone before and after the contact region is indicated by a blue color in part (a) and exhibits a strain value of – 2.84 mm. It is noteworthy that the piezoelectric element is exposed to a small amount of stress in the unloading zone, which can produce some energy before and after the loading region. Same Fig. 14a shows a change in tire width in the contact region, where tw1 represents the inflated static tire width and tw_2 represents the deformed tire width during steady-state rolling. The difference between tw_1 and tw_2 comes from the stress applied on the tire at the contact region.

Figure 14b indicates that the optimal tire footprint width along the lateral direction is 53.621 mm. Therefore, the maximum width of the TSPEH structure should not exceed 53.621 mm to maintain the applied strain at the maximum level of 16.711 mm.

Similarly, Fig. 14c shows the optimal tire footprint length along the longitudinal direction, which is 50.2 mm. Thus, the maximum TSPEH structure length should not exceed 50.2 mm for maximum performance.

Tire stress analysis

The tire imprint (tire footprint) is the only region of contact between the tire and pavement where contact stress occurs. The size of the tire–pavement contact area increases with increasing load applied to the tire [55]. Changing the tire inflation pressure is another factor that affects the size of the contact patch [56]. The tire–pavement region is usually assumed to be circular or rectangular, but in reality, stress is not spread evenly across the contact zone. During rolling, the lateral stress in the imprint zone is higher than the longitudinal and transverse contact stresses because the lateral strain of the tire is usually greater than the longitudinal and transverse strains [57].

Figure 15 shows the stress contour plot for different stress components for the tire cross-section at the center of the tire–pavement contact region. From the Fig. 15a, it can be noted that the maximum von Mises stress 1.301 MPa occurs in the steel belts below the shoulders. Figure 15b indicates that the maximum stress is 0.662 MPa located at the tire tread. Figure 15c shows the maximum stress of 0.275 MPa at the sidewall close to the rim due to the strain applied in this region. Figure 15d demonstrates the maximum stress of 0.559 MPa in the contact region, which occurs along the tire sidewall due to the vertical load applied to the tire. Therefore, the stress amount of 0.559 MPa is considered as the primary tire stress value that is directly applied to the TSPEH.

Transducer simulation

The initial design of the harvester was simulated using the COMSOL Multiphysics software. All the parameters and dimensions were set based on the analysis of the tire and previous literature. To ensure the proper design of the energy harvester, various parameters were carefully selected based on previous research and analysis. Specifically, the

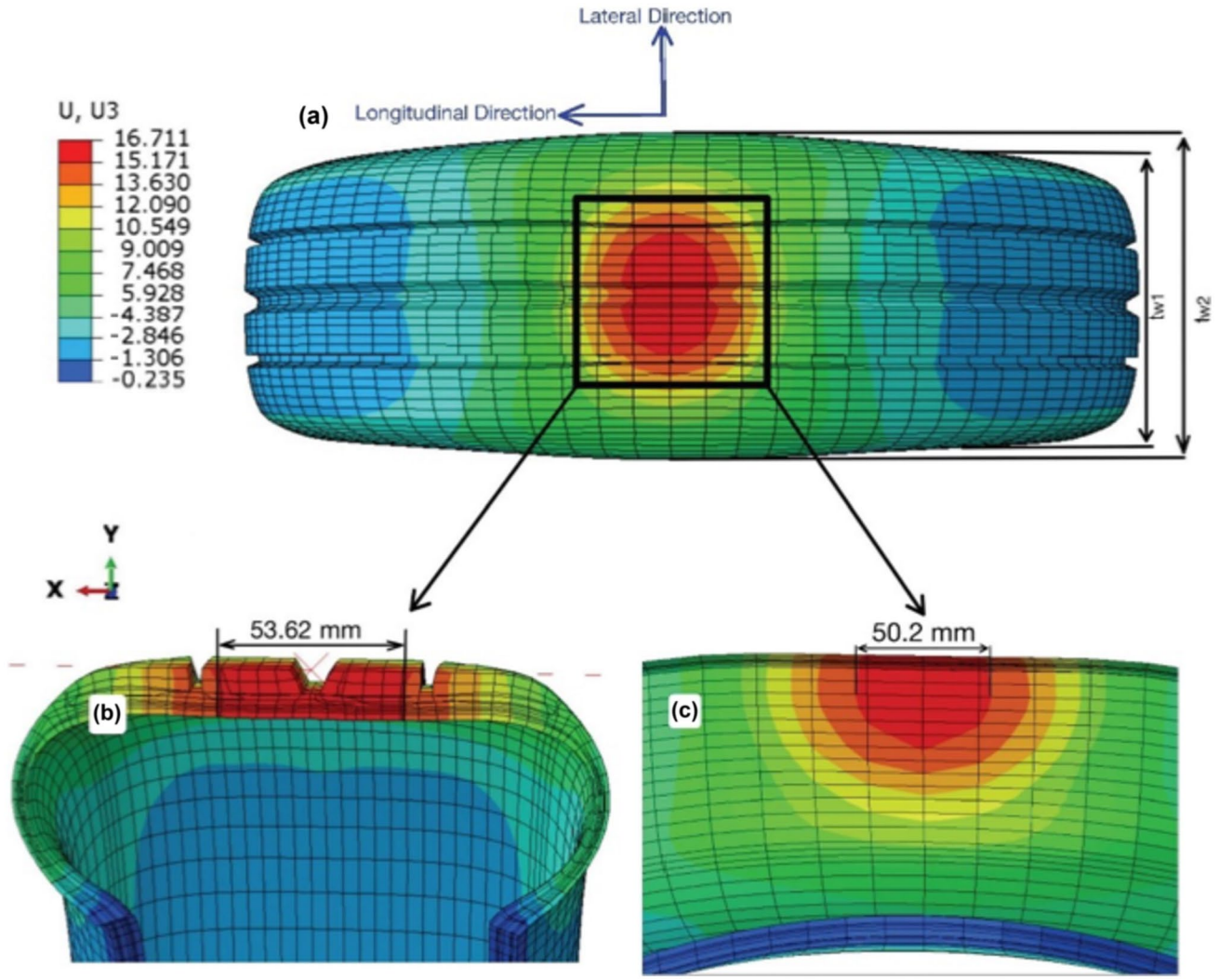

Fig. 14 **a** The maximum strain area at the tire contact region (b) contact region width for maximum strain **b** contact region length for maximum strain

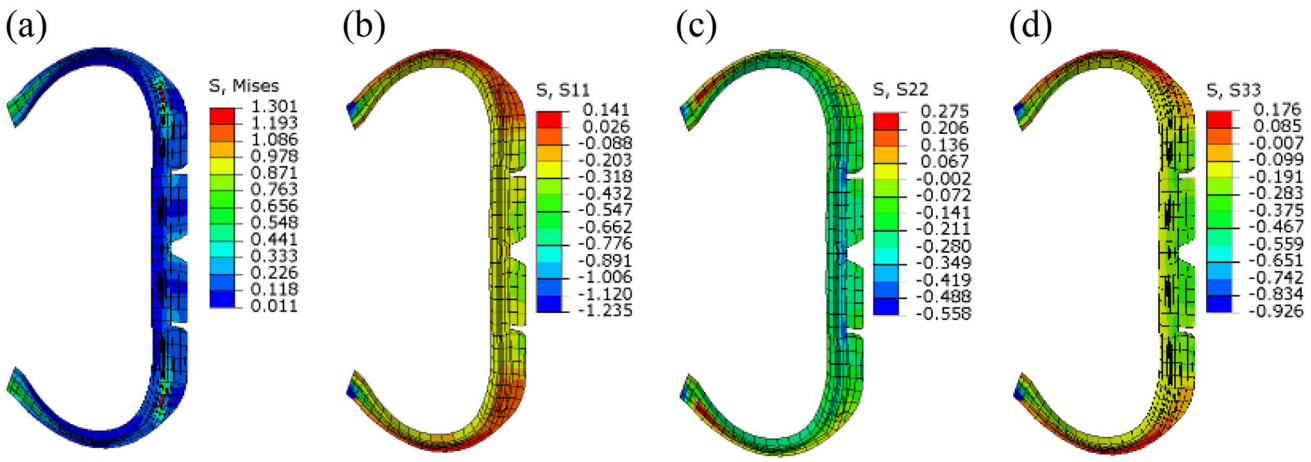

Fig. 15 Stress nephogram of the tire–pavement contact model. **a** Von mises stress nephogram. **b** Stress nephogram of S1 along the tread. **c** Stress nephogram of S2 along the side wall. **d** Stress nephogram of S3 of the tire contact region

length of the harvester was determined by considering the calculated contact patch dimensions, while the thickness of the piezoelectric material was selected based on information from prior literature. Moreover, to ensure precise and secure installation of the harvester, the end cap radius was set at 351 mm, which matches the radius of the proposed tire (175/65 R14) used in this study. This approach is to ensure a perfect fit and proper mounting of the harvester within the tire structure. The primary objective of the harvester modeling was to determine the amount of energy that the harvester could generate.

As the harvester is intended to be mounted inside a vehicle tire, the properties of the tire's inner environment, such as tire stress and rotation frequency, were set as the input boundary conditions when simulating the harvester using the COMSOL Multiphysics software. The bottom boundary of the harvester structure is the only connection between the tire and the transducer structure. In previous studies, the entire bottom boundary area was adhered to the tire inner wall using epoxy material. However, the main drawback of this adhering method is that only 25% of the tire strain can be transferred to the harvester due to the high stiffness of the epoxy. Full details of the TSPEH installation methods can be found in [16].

In this study, the bottom layer of the harvester structure was designed to be free and not glued to the tire rubber. The only adhered regions from the TSPEH to the tire are the two external boundaries of the aluminium substrate base. This condition is similar to a beam that is fixed from both ends. This installation method is proposed to tolerate 100% of tire strain to be transferred directly to the harvester bottom layer, thereby producing a higher energy. Another advantage of this mounting approach is that the tire stiffness would not be affected by an epoxy layer, eliminating any tire safety concerns. Figure 16 represents the initial recommended dimensions that were selected based on previous studies, tire analysis findings, and COMSOL pre-tests.

The electrical circuit used in this study for the TSPEH is presented in Fig. 17. The circuit consists of a piezoelectric material serving as a voltage source, a bridge diode rectifier, a capacitor, and a resistor. The piezoelectric material generates an AC voltage, which is converted to DC voltage

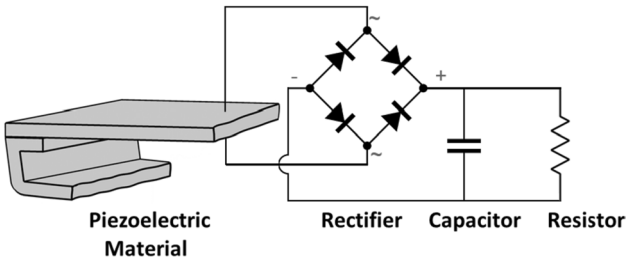

Fig. 17 TSPEH electrical circuit

through the rectification process. This electrical circuit is a single-stage powering system that charges a single capacitor. Its main purpose is to evaluate the electrical performance of the harvester. In future studies, potential enhancements to the circuit may include the addition of a second capacitor that can be charged after the first one, as well as a voltage regulator for optimal performance.

To evaluate the performance of the M_1 model, two loading modes were applied using COMSOL Multiphysics software: tire loading mode and linear stress loading mode. It was assumed that the transducer structure would bear 100% of the host load for design purposes.

Tire boundary condition loading mode

The first loading mode applied to the TSPEH M_1 involved imposing tire boundary conditions in COMSOL Multiphysics, as summarized in Table 6. In this study, the von Mises stress distribution was analyzed and the results showed that there is stress concentration along the edge of the substrate base structure, as illustrated in Fig. 18a. Additionally, the deformation pattern of the end cap was found to resemble the behavior of the tire deformation at the point of contact with the road due to the applied tire stress. This is important as it ensures a perfect bonding inside the tire, leading to higher deformation cycles and a longer lifespan. The minimum stress distribution was at the piezoelement, as the end cap absorbed most of the tire high stress and converted the large portion of it to horizontal stress applied to the piezoelement. This would increase the piezoelement energy production and

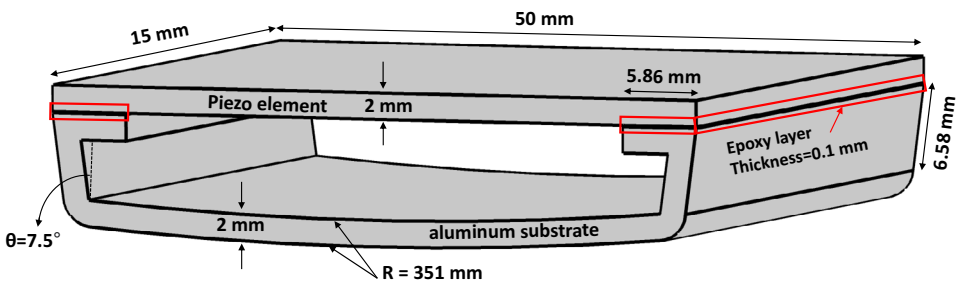

Fig. 16 Initial dimensions for the harvester structure (M_1)

Table 6 COMSOL Multiphysics boundary conditions of TSPEH analysis

Boundary Conditions	Description	Value
Solid Mechanics B.C	PZT-5X width (based on Fig. 14)	15 mm
	PZT-5X length (based on Fig. 14)	50 mm
	PZT-5X material thickness	2 mm
	Tire contact region impact frequency (based on 74.04528 rad/s tire angular velocity)	11.78 Hz
	Tire loading mode: stress applied to Harvester (based on Fig. 15d)	0.559 MPa
	Linear loading mode: stress applied	0–2 MPa with 0.1 MPa interval
	Coordinate system of polling direction for PZT-5X	Polled along material thickness
	Piezoelectric material constitutive relation	Strain-charge form
	Aluminium and epoxy solid model	Isotropic linear elastic material
Electrical B.C	PZT-5X dielectric model	Relative permittivity
	Lower surface of the PZT-5X	Ground electrode
	Upper surface of the PZT-5X	Terminal electrode
	Resistance	1E5 to 1E6
	Capacitance	100 nF
	Rectification bridge diode	1N4007 type

lifespan. In previous DECEH models, the maximum stress could occur at the adhesive boundary between the piezoelectric material and the aluminum substrate, causing early failure to the harvester structure. However, in this model, the adhesive layer area is large enough to distribute stresses in that region.

Since the piezo is vertically polarized along its thickness as stated in Fig. 3, Fig. 18b, c illustrates the front and side view of voltage distribution between the upper and lower piezoelectrodes. The maximum open circuit voltage is + 291 V that is distributed on the external boundaries of the piezo while the negative charge of – 292 V located in the piezoelement center. This distribution of voltage is due to the fact that the piezo is subjected to mechanical stress and strain that causes the charges to accumulate on its external surfaces. The compression and tension zones within the piezo-material play a role in creating this stress or strain and therefore contribute to the distribution of the voltage and charge in this way. For example, the piezoelement area that adhered to the end cap usually compressed while the remaining piezoelements usually stretched horizontally and bent slightly.

Regarding the electric field, Fig. 18d, e shows the front and side views of the electric field distribution for the piezoelement. The maximum electric field occurs near the upper and lower electrodes, with a value of 676 kV/m, while the minimum electric field density was at the piezo-area that adhered to the end cap, with a value of 2.76×10^{-4} kV/m. It can be noted that increasing the adhered area of the piezoelement would assist in reducing stress concentration at the contact edges between the piezo and the end cap, but it would decrease the electric field density. The piezoelement area that are adhered to the end cap are only subjected to compression, which targets the d31 mode. This is unlike the other area of same piezoelement that are simultaneously tensioned and bent, triggering both d31 and d33 modes, resulting in greater energy harvesting. Hence, to achieve optimal results, a balance between design limitations and energy output must be carefully considered.

Linear stress loading mode

External loads applied on tires vary each time due to road bumps, rough roads, and the number of passengers in the vehicle. To examine the transducer's behavior and efficiency under higher loads, stress was applied in the range of 0–2 MPa, representing a linear increase in the applied load on the transducer substrate. The same boundary conditions were applied as the first loading mode, except for the amount of the applied stress, which previously was 0.559 MPa for the tire boundary loading scenario.

When the transducer pursued a 2 MPa load, the maximum von Mises stress was equal to 617 MPa at the edge of the substrate structure, as shown in Fig. 19a. This is due to the bending that occurs at the base boundary of the aluminum substrate. When the load increased four times compared to the tire scenario, the maximum von Mises load also increased four times. This indicates that the increase in external load can be considered equal to the increase in internal structure stress, which can be beneficial during the design process.

Similar to von Mises behavior, the voltage increased linearly with respect to the applied load, as shown in Fig. 19b. The maximum open-circuit voltage was equal to 768 V at

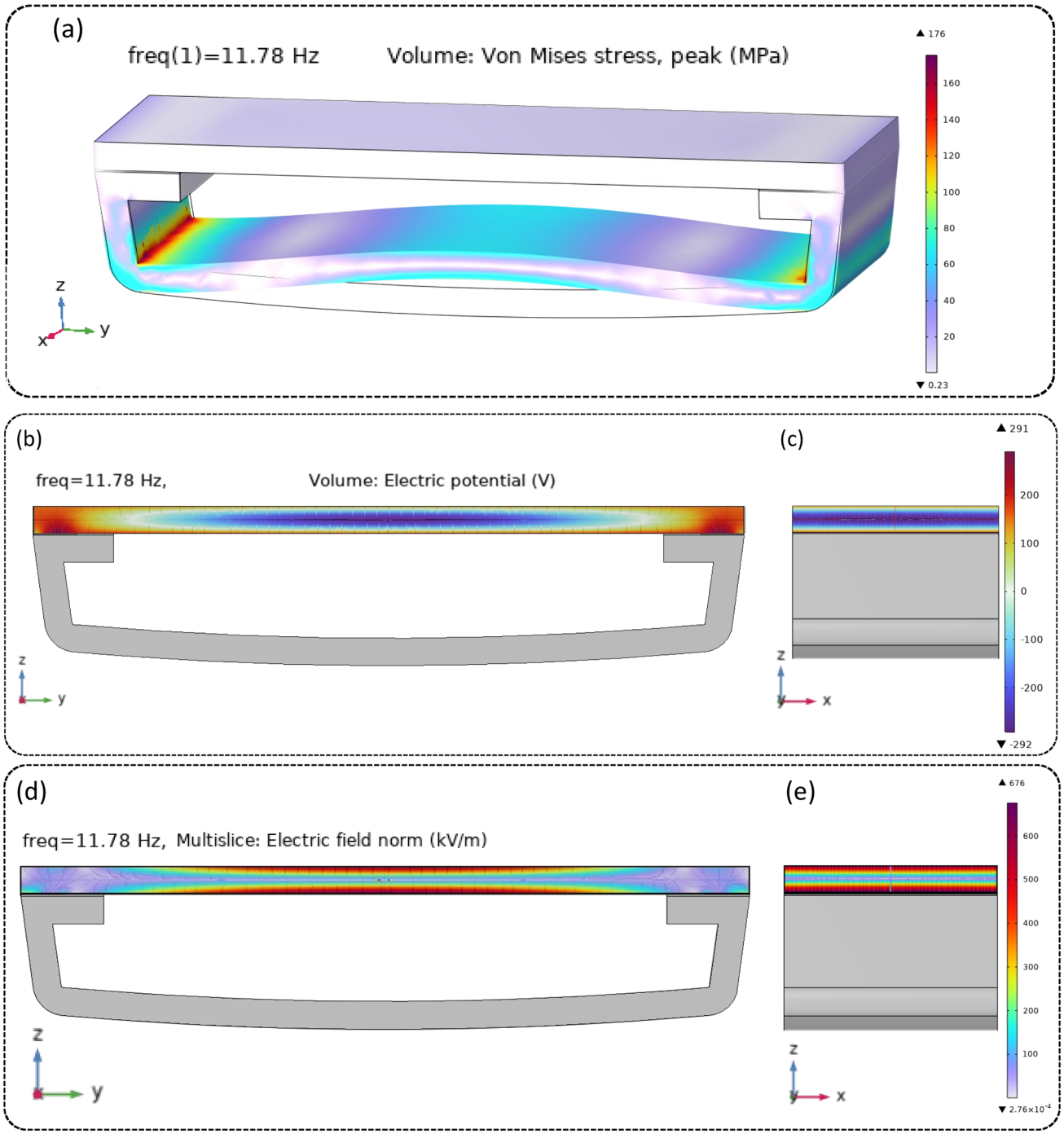

Fig. 18 TSPEH analysis when applying rolling tire boundary conditions. **a** Von Mises stresses and substrate deflection. **b** Front view of piezo-voltage. **c** Side view of piezo-voltage. **d** Front view of electric field. **e** Side view of electric field

a load of 2 MPa. Since the relationship between load and voltage is linear, the transduced voltage can be predicted for untested loads. Therefore, it is expected that the voltage would increase in the same manner if the stress increased beyond 2 MPa. However, the maximum applied stress should be less than the maximum allowable load to avoid structure failure.

The voltage distribution along the piezoelement was similar to the voltage distribution in the tire loading condition, as shown in Figs. 19c, d for the front and side view electric potential, respectively. The positive charges tended to locate at the external piezo-boundaries, while the negative charges concentrated in the middle. This was due to internal piezo-stresses affecting voltage distribution due to

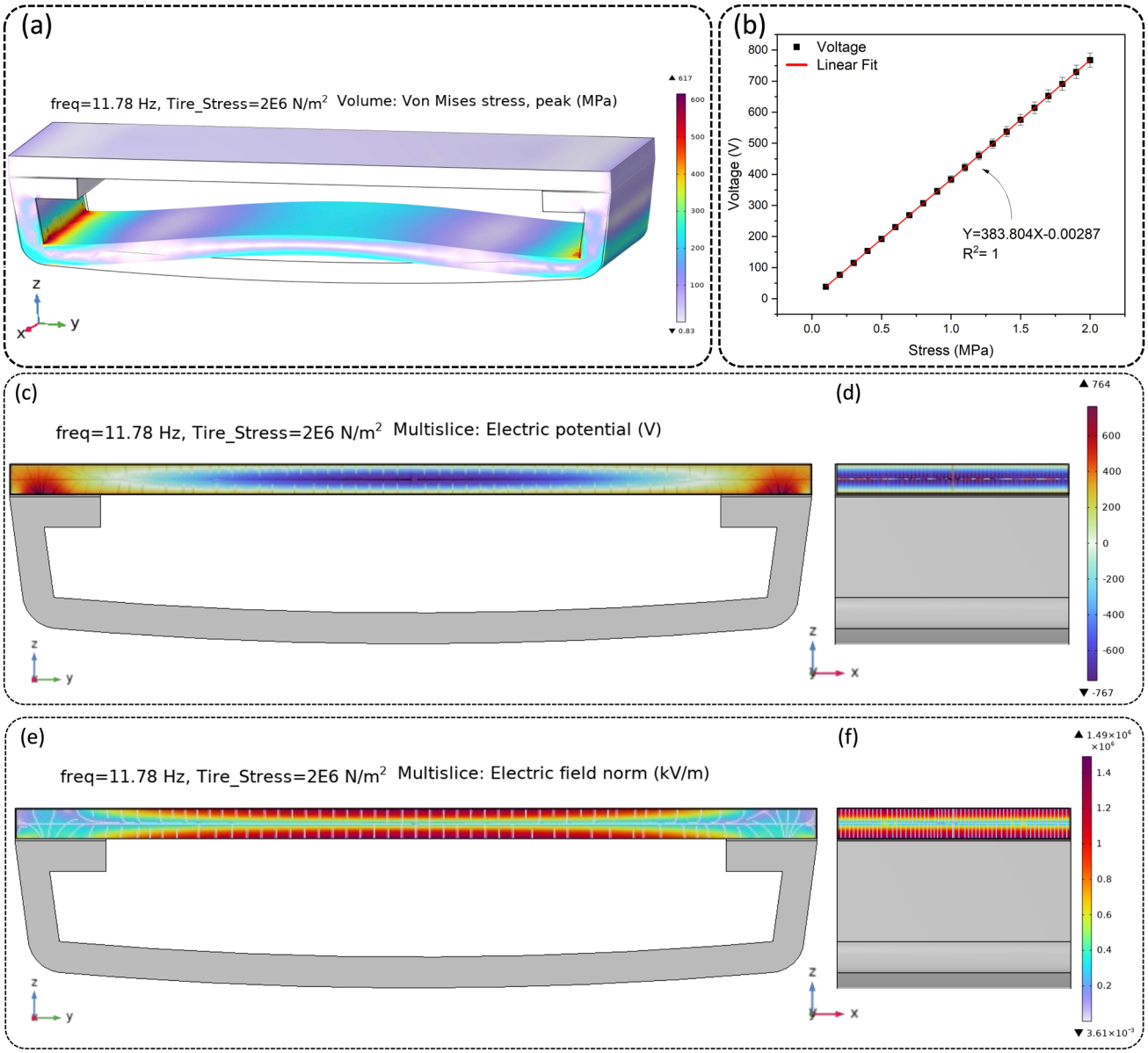

Fig. 19 TSPEH analysis at 2 MPa applied stress. **a** Von Mises stresses and substrate deflection. **b** Open circuit electric potential (V) for M1 under (0–2) MPa applied stress. **c** Front view of piezo-voltage. **d** Side view of piezo-voltage. **e** Front view of electric field. **f** Side view of electric field

structure deformation. The adhered piezo-region showed a higher voltage compared to the rest of the piezoelement, possibly due to the direct stresses transferred from the end cap to the piezoelement. The adhered piezo-region experiences compression stress that is parallel to the polling direction, triggering the d_{33} piezoelectric coefficients more than the d_{31} coefficients. The d_{33} piezo-coefficient is higher than d_{31}, which results in more voltage being transduced from this region.

The front and side view of electric field density for the piezoelement is represented in Fig. 19e and Fig. 19f respectively. The maximum voltage density was close to the upper and lower electrodes with a value of 1.49×10^6 kV/m, while the minimum electric field density was at the piezo-area that adhered to the end cap, with a value of 3.61×10^{-3} kV/m.

The piezoelectric effect governs the connection between voltage and electric field in piezoelectric materials. When mechanical strain is applied to a piezoelectric material, it generates an electric field that induces a voltage across the substance. The intensity of the electric field is proportional to the amount of mechanical strain given to the material, and its direction is determined by the direction of the mechanical strain. It was observed in this study that the regions with the greatest voltage had the lowest electric field and vice versa.

This is explained by the nonlinear piezoelectric response of the PZT-5X material. The material has a high piezoelectric coefficient and a low dielectric constant at low strain levels, resulting in a low electric field and a high voltage output. As the strain level increases, the piezoelectric coefficient decreases and the dielectric constant increases, which leads to a higher electric field and a lower voltage output. As a result, the regions with the highest voltage value are expected to have a lower electric field since they correlate to low strain levels where the material has a high piezoelectric coefficient. The locations with the lowest voltage value, on the other hand, would have a stronger electric field since they correspond to high-strain levels where the material has a low piezoelectric coefficient. This behavior is typical of PZT-5X and corresponds to the piezoelectric properties of other comparable materials.

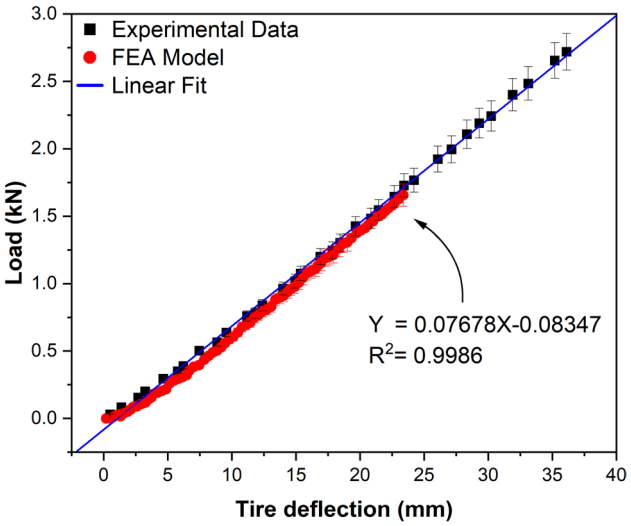

Fig. 20 Tire force–displacement profile validation for static tire model compared with Kubba et al.'s study [18]

Validation

Tire model validation

The output of the Abaqus tire simulation must be validated against experimental data as a reference strain value. However, collecting experimental data is a time-consuming and costly process. To address this, the tire model's static analysis compared with the experimental results of Kubba, Behroozi [18], who used the same tire size (175/65 R14) and boundary conditions as this study. During Kubba et al.'s experiment, a 2.7 kN radial load was applied to the full tire specimen, while this study considered only 1650 N for a half 3D tire model simulation. This is because simulating a full tire 3D model requires 50 to 100 times more elements than a 2D model, which is an expensive and time-consuming approach. Figure 20 shows the tire load–deflection curve comparison between this study and Kubba et al.'s experimental results.

The tire deflection demonstrated a linear response to the applied radial load within the load range of 0 N to 1.65 kN, as depicted in Fig. 20. This indicates a proportional relationship between the radial load and the resulting tire deflection within the specified range, demonstrating predictable and consistent behavior of the tire. Specifically, small changes in the applied load will result in corresponding small changes in tire deflection, in direct proportion to the change in load.

The linear relationship between load and deflection is an important characteristic of tire behavior, allowing for accurate prediction of tire performance under varying loading conditions. Comparison of the tire model used in this study with Kubba et al.'s experimental results shows good agreement, with a maximum error of 1.22%. This finding is significant as it provides evidence that the tire model employed in the simulation accurately captures the linear relationship between load and deflection observed in experimental results. Such validation of the tire model is essential to ensure its usability for further analysis and prediction of tire performance under varying loading conditions.

TSPEH model validation

Existing studies on bridge-shaped transducers cannot be used for validation reasons due to the originality of the transducer structure explored in this research. This is due to the fact that the investigated structure consists of a single end cap that is bonded to the tire's inner liner.

To solve this issue, the model was converted into DECEH by copying and mirroring the end cap and adhesive in the Z-axis. This is to generate a validation structure more closely matching typical bridge transducers with two end caps, as illustrated in Fig. 21a.

Figure 21a shows the M2 model, which is identical to the M1 model except for the inclusion of upper and lower end caps that compress the single piezoelectric element. The same boundary conditions were employed for implementing the M2 model. The main difference between this model and the M1 model was the imposed stress. The M1 model has a single stress applied to the lower cap, whereas the M2 model has stress (0–1 MPa) applied to both the lower and the higher end caps. The arc bridge transducer has a similar form to this research harvester.

The open circuit voltage for M_2 was compared to the Li study [22], as illustrated in Fig. 21b. The incorporation of error bars in Fig. 21b shows a comparative analysis of this study's outcomes and Li's experimental results. Notably, the error bars stay minimum within the stress range of 0–0.5 MPa, which is similar to the comparison range versus Li's experimental results. As a result, this agreement

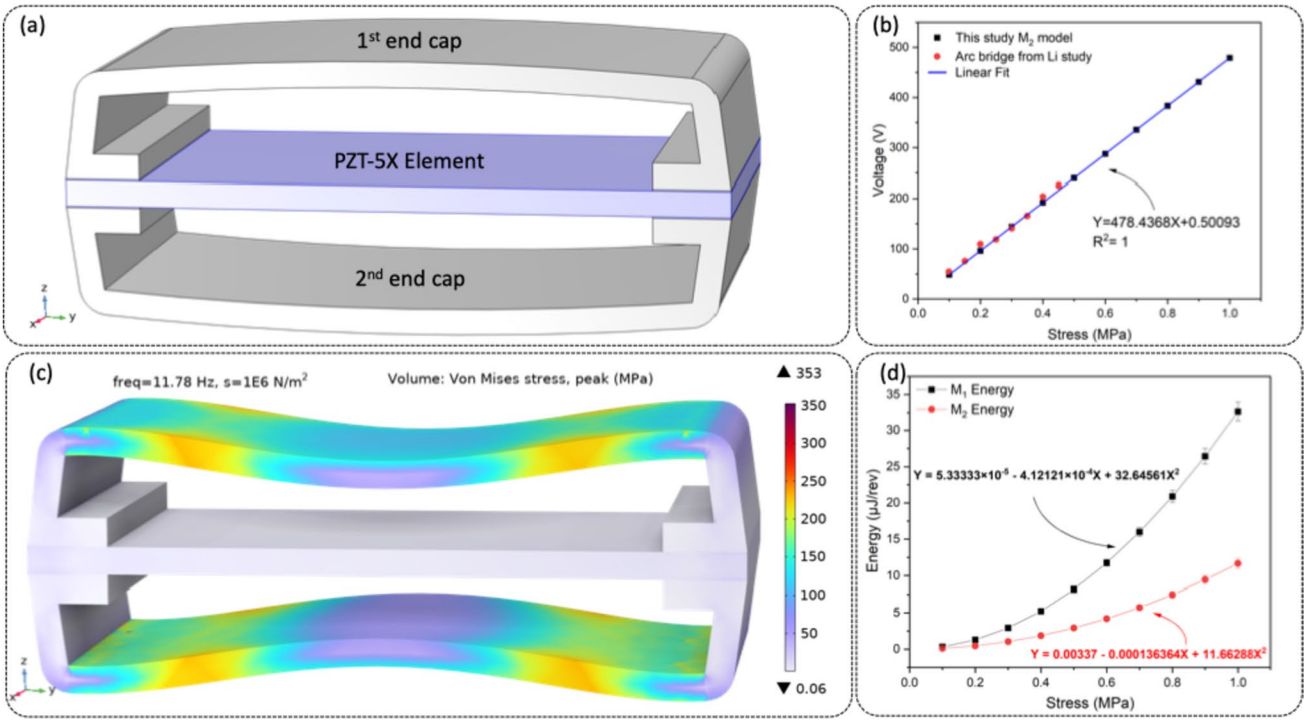

Fig. 21 DECEH M2 **a** Transducer model **b** M2 model transduced voltage compared to Li study [22]. **c** Von Mises Stresses and substrate deflection **d** harvested energy comparison for M1 and M2 models of this study

supports the validity of the comparison. However, beyond the 0.6 MPa stress, there is a small rise in error bars. Despite such an increase, the errors remain within an acceptable range, as illustrated in Fig. 21b.

The harvested voltage increases as applied stress increases for M_2 model and Li study. Under one MPa applied stress, the voltage of the M_2 model reaches 478.94 V. Under 0.45 MPa applied stress, the arc bridge from Li's study produced a maximum voltage of 220 V. This is because the arc bridge in their study failed at 0.5 MPa, whereas the M_2 model in this study performed normally under 1 MPa applied stress. The voltage profile for the M2 shows a very good agreement with the arc bridge voltage presented by Li study. Therefore, the simulation results can be considered as a valid finding.

Figure 21c depicts the deformed M2 model. Because of the imposed load on both end caps, the maximum von Mises stress of 353 MPa occurs at the two end caps. The largest stress occurs away from the piezoelectric element, notably on the end caps, as in the M1 model scenario. This is practical because if the maximum von Mises stress occurs on the piezoelement, it will break faster than if it occurs on the end cap element because the aluminum end cap is considerably more flexible than the fragile PZT-5X element.

The harvested energy of both the M1 and M2 structures is presented in Fig. 21d. The collected energy for the M1 model under the tire boundary condition was 10.201 μJ/rev, while the highest energy was 32.645 μJ/rev under a load of 1 MPa. It is worth pointing out that under the same applied stress, the M2 model produced less energy than the M1 model. Under a stress of 1 MPa, the maximum energy collected by the M2 model was 11.666 μJ/rev. This is because, despite the fact that dual end cap energy harvesters such as the M2 can withstand higher stresses, they are usually stiffer and hence produce less energy than one-end cap energy harvesters similar to the M1 in this study, which has more flexibility accounting for its triple energy.

Tire strain experimental measurement

Due to their high flexibility, piezo-strain sensors are one of the solutions that are frequently employed to calculate tire strain. The LDT2-028K Polyvinylidene Fluoride (PVDF) Strain Sensor is often used to monitor tire strain. This is because it can transform the applied mechanical stress or strain into an electrical charge. Three strain sensors are employed simultaneously to monitor tire strain for precise results.

Three Sensors of LDT2-028 K installed to the inner liner of the 175/65 R14 tire at 135°, 180°, and 225° angles. The reason for choosing these angles for positioning the sensors is because of the tire contact patch two compression and one tension zones. To accurately define these locations,

the tire external and internal circumferences were measured then divided by 360° as seen in Fig. 22a. Then the sensors mounted inside the tire using a strong adhesive tape as depicted in Fig. 22b. However, taping the sensors inside tire was not successful because the tape removed after few tire rotations due to high tire pressure, rotation, and vibration. Therefore, a filled epoxy resin (X238) used to fix the sensors in place by adhering the sensors on the center of the marked positions as illustrated in Fig. 22c, d. This method works well that perfectly mount the sensors into tire inner liner until completing the tire tests.

After mounting the sensors inside the tire, the data wires were connected to the data acquisition system (DAS). The tire was mounted on Chevrolet Aveo 2006 with axle weight of 330 kg. The test was conducted at the School of Mechanical Engineering, USM at a speed of 20, 40, and 80 km/h as illustrated in Fig. 23. Measurements were taken at constant Driving speeds.

The strain sensor voltage was 6 V peak to peak at a speed of 20 km/h. Due to difference in sensors locations, there were a time difference between them. The time difference between each reading was constant. The voltage reading and trend was similar for all three sensors as illustrated in Fig. 24 below.

To examine the effect of vehicular speed on the strain sensor signal, three vehicle's speeds were conducted namely 20, 40, and 80 km/h. The output signal voltage was not influenced by the tire frequency. This finding agreed well with other researchers who stated that the tire RPM does not affect the tire deformation. This is due to the fact that the tire deformation is mainly influenced by the vehicle weight or external load applied on tire. Figure 25 below depict the signal of one strain sensor under different vehicle speeds.

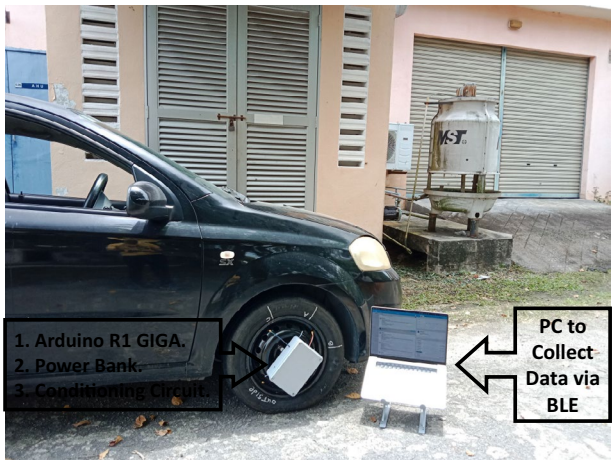

Fig. 23 Tire Strain Measuring Method

Compare energy output with other studies

Since there is no similar harvesting structure related to this study, transducing structures that consist of a flexible substrate and piezoelectric material from other researchers were used for energy comparison purpose. The piezoelectric energy harvesters from other studies produced energy in the range of 40 µW–6.5 mW [58]. Table 7 shows the performance of the TSPEH compared to other transducers. Although the energy produced in this study was lower than other studies, it is important to note that other DECEH harvesters were designed to withstand very high stresses and low deformation, unlike the TSPEH which was designed to be flexible to not affect tire flexibility

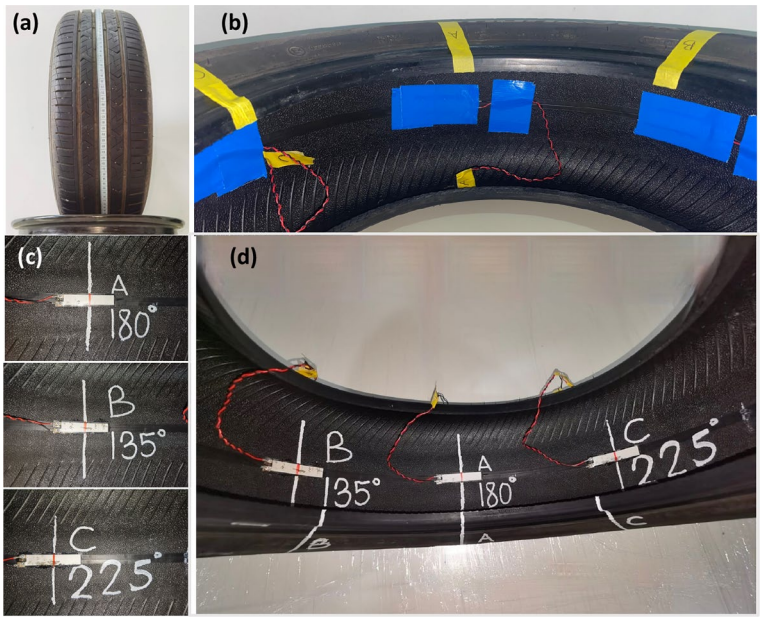

Fig. 22 Strain Sensor Installation Techniques **a** circumference measurement **b** sensors mounting using tape **c** adhering sensors using epoxy **d** full installed sensors

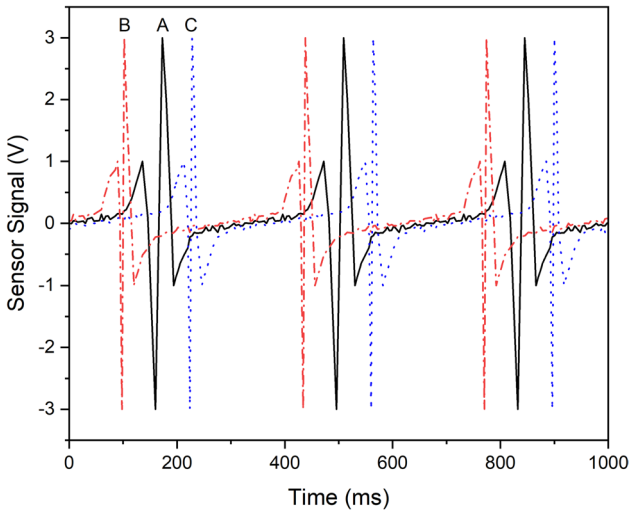

Fig. 24 PVDF tire strain signal from three different sensors 20 km/h

and safety, and to provide a longer lifespan for the brittle piezoelement structure that installed in a rough tire environment. Another point to consider is that other researchers often use very high resistive loads which are usually higher than real TPMS applications, which means the power presented in their studies is not always realistic due to the high resistive loads.

Calculate sensors number in each tire

After energy output was found, calculating number of sensors that can be powered in each tire are essential. The power consumed by a sensor depends on the rate of signal transmissions per minute. A typical TPMS sensor consumes 120–450 μW at a transformation rate of 10–60 samples per minute [18]. Energy demand for a wireless sensor for each tire rotation could be calculated using equation below [61]:

$$E_{\text{rev}} = n_{\text{samples}} \times n_{\text{axes}} \times 50pJ + \left(n_{\text{bits}} + 10\right) \times 10 \text{ nJ}, \quad (13)$$

where n_{samples} , n_{axes} , andn_{bits} are transmission rate per revolution, axis number from which data is collected, and the number of transmitted bits, respectively. Usually commercial TPMS sensor consumes about 10 μJ/rev [7]. Due to its ability to collect 32.645 μJ/rev, this research M_1 structure can power up to 3 commercial sensors. The harvested energy can be further increased using higher capacitors such as super capacitors. Additionally, since this TSPEH's width is only 15 mm, it can be stacked as three within the same spot, producing a total energy of 98 μJ/rev.

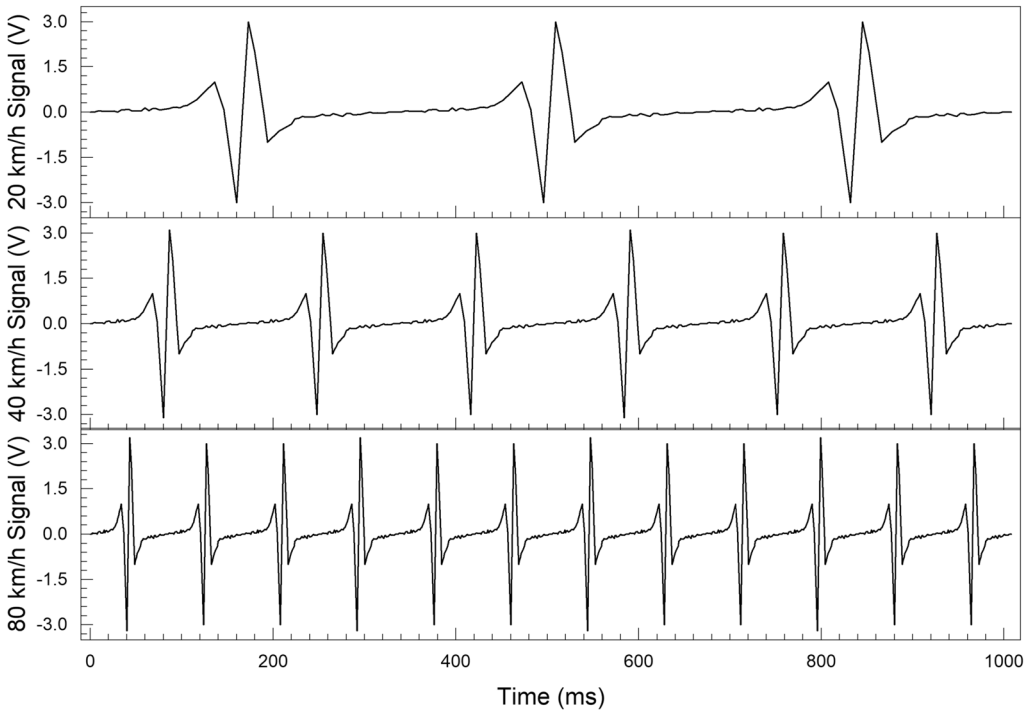

Fig. 25 PVDF tire strain signal from three different sensors at various vehicle speeds

Table 7 TSPEH performance comparation with reference to other transducers

Authors	Objective	Design specifications		Major findings	
		Specimen design	Test scenarios	Electric output	**Conclusions**
Yao et al. [21]	Comparing Arc and trapezoidal bridge transducers for asphalt pavement applications	PZT-5H supported by 30×20×2 mm of Arc and trapezoidal bridge transducers	0.5 to 3.5 kN load 15 and 20 Hz load frequency	Maximum voltage of 106 V for trapezoidal bridge Maximum voltage of 232 V for arc bridge	The arc bridge transducer was broken at 0.45 MPa stress. However, arc shaped transducer showed a higher voltage output than the trapezoidal bridge transducer
C. Li [22]	Comparing of energy transduction efficiency for arc and rectangular bridge transducers	PZT-5H Piezoelectric Plate with size of 30×20×2 mm	0.1 to 0.7 MPa stress applied 1 Hz and 5 Hz load frequency	Maximum voltage of 160 V for rectangular bridge Maximum voltage of 220 V for arc bridge	Under same loading conditions, arc bridge transducer shows a 40% higher voltage
Yesner et al. [59]	Harvest traffic loading energy on pavement using horizontally poled PZT-5X material	64 bridge transducers of 32×32×2 mm^3 PZT-5X	5 Hz 400 K Ohm 500 lb loading force	2.1 mW power 2.15 kV/mm electric field between electrodes	Linear relation between applied force and resulted voltage was found
Lee et al.[60]	Powering tire sensors from wasted tire strain	60×14×0.8 (mm) of PZT-5H interdigitated electrodes	450 kgf load 60 km/h velocity	380 mJ energy 4.05 mW/mm^3 power density	The thickness of the piezo material has greater influence on produced energy compared to applied load and tire velocity
Esmaeeli et al. [13]	Improve energy efficiency of the tire mounted transducer	Rainbow shaped structure consist of two piezo materials separated by a flexible substrate	2500 kg car weigh 41 km/h velocity	9.7 V voltage 5.85 mW power 95 µJ/rev energy	Increasing piezo width from 2.5 to 8.5 mm increases energy efficiency from 0.69 to 8.3%
Aliniagerdroudbari et al. [20]	Amending cymbal shape harvester to provide sufficient energy to power tire sensors	Cymbal shape piezo with a diameter of 5 mm supported by two legs structure	Force of 500 kgf Speed of 41 km/h	7 V voltage 5 mW power 90 µJ/rev energy	The transduced energy is sufficient to power 9 TPMS
Jasim, Wang [26]	Design optimization of Multi-poled bridge transducer	32×32x2 Square PZT-5X element	0.7 MPa loading	556 V, 0.743 mJ potential energy for open circuit	Steel end cap thickness and cavity height have a more influence on the resulted stresses than geometrical parameters
This study TSPEH models (M_1 & M_2)	Design a new energy harvester and evaluate its energy output for tire applications	A PZT-5X adhered to a flexible aluminum substrate 50×15×2 (mm)	The rolling tire boundary condition 11.78 Hz 0.559 MPa applied stress	214 V Tire boundary condition & 768 V under maximum stress of 2 MPa 10.201 µJ/rev energy under tire B.C. & 32.645 µJ/rev energy under 1 MPa stress	One to three TPMS sensors can be powered by the novel one-end cap TSPEH

Conclusion

This study designed a novel one-end cap tire strain piezoelectric energy harvester (TSPEH) under different loading modes. The decoupled modeling approach was used to analyze the interaction between the tire and energy harvester, and the transducer's dimensions were established based on tire analysis. The results revealed that stress concentration occurred along the edge of the end cap. Under changeable loads, the maximum von Mises stress and open-circuit voltage increased linearly with respect to the applied load. Considering the balance between design limitations and energy output to achieve optimal results, under normal tire load scenarios, the TSPEH was able to generate a voltage of 291 V, while a maximum voltage of 768 V was harvested under a 2 MPa tire contact patch stress. Based on a 10 μJ/rev sensor consumption rate, up to three commercial TPMS can be powered by this TSPEH, which generates 32.645 μJ/rev. Due to the lack of sufficient information about one-end cap tire strain energy harvesters, experimental work will be conducted later based on a sound theoretical foundation that includes more analysis for tire-harvester interaction and harvester geometrical optimization for maximum reliability and efficiency. Overall, this study shows that one-end cap piezoelectric energy harvesters have great potential as a promising source for sustainable energy harvesting in various applications, notably in utilizing wasted host energy such as vehicle tires.

Acknowledgements The authors would like to acknowledge Dr. Ammar I Kubba, Al-Naharain University, Iraq for his support during tire analysis.

Author contributions AJ proposed research concept and study plan and revised paper draft; IAl-N conducted numerical simulation and experimental work and wrote paper draft; KWC and S-YP provided comments to data analysis and paper draft.

Data availability The datasets that support results are obtained from experimental work which was performed in the lab., so data are already available and can be found directly in the manuscript.

Declarations

Conflict of interest The authors declare that they have no known competing financial interests or personal relationships that could have appeared to influence the work reported in this paper.

References

1. Aljendy, R., et al.: A novel optimisation method for optimal integration of the hybrid distributed generation with FACTS device: a practical case study. Int. J. Power Energy Convers. **12**(4), 314–337 (2021)
2. Yesner, G., et al.: Evaluation of a novel piezoelectric bridge transducer. In: 2017 Joint IEEE International Symposium on the Applications of Ferroelectric (ISAF)/International Workshop on Acoustic Transduction Materials and Devices (IWATMD)/Piezoresponse Force Microscopy (PFM). IEEE (2017)
3. Allamy, W.K.J., & Al-Najati, I.A.H.: A thermal insulator manufacturing, using solid residuals from pulp and paper factories in Missan City. In: AIP Conference Proceedings, **2338**(1). AIP Publishing (2021)
4. Reina, G., Gentile, A., Messina, A.: Tyre pressure monitoring using a dynamical model-based estimator. Veh. Syst. Dyn. **53**(4), 568–586 (2015)
5. Mishra, S., Liang, J.-M.: Design and analysis for wireless tire pressure sensing System. In: New Trends in Computer Technologies and Applications: 25th International Computer Symposium, ICS 2022, Taoyuan, Taiwan, December 15–17, 2022, Proceedings. Springer (2023)
6. Berger, N., et al.: Risk management of supply chain disruptions: An epidemic modeling approach. Eur. J. Oper. Res. **304**(3), 1036–1051 (2023)
7. NHTSA. Vehicle Safety Research. Accessed 2 April 2023: National Highway Traffic Safety Administration.
8. Iclodean, C., Varga, B.O. , Cordoș, N.: Safety and cybersecurity. In: Autonomous Vehicles for Public Transportation, pp. 139-165. Springer (2022)
9. Jasim, A.F., et al.: Performance analysis of piezoelectric energy harvesting in pavement: laboratory testing and field simulation. Transp. Res. Rec. **2673**(3), 115–124 (2019)
10. Wang, H., Jasim, A.: Piezoelectric energy harvesting from pavement. In: Eco-Efficient Pavement Construction Materials, pp. 367–382. Elsevier (2020)
11. Shakir Radeef, Z.: Design of a piezoelectric generator for vibration energy harvesting using non ferroelectric PZnTNT/Zainab Shakir Radeef (Doctoral dissertation, University of Malaya). (2018)
12. Esmaeeli, R., et al.: Design, modeling, and analysis of a high performance piezoelectric energy harvester for intelligent tires. Int. J. Energy Res. **43**(10), 5199–5212 (2019)
13. Esmaeeli, R., et al.: Optimization of a rainbow piezoelectric energy harvesting system for tire monitoring applications. In: Energy Sustainability. American Society of Mechanical Engineers (2018)
14. Yang, Z., et al.: High-performance piezoelectric energy harvesters and their applications. Joule **2**(4), 642–697 (2018)
15. Lee, J., et al.: A self-powering system based on tire deformation during driving. Int. J. Automot. Technol. **13**(6), 963–969 (2012)
16. Al-Najati, I.A.H., Chan, K.W., Pung, S.-Y.: Tire strain piezoelectric energy harvesters: a systematic review. Int. J. Power Electron. Drive Syst. (IJPEDS) **13**(1), 444–459 (2022)
17. Makki, N., Pop-Iliev, R.: Pneumatic tire-based piezoelectric power generation. In: Active and Passive Smart Structures and Integrated Systems 2011, vol 77, pp. 186–198. SPIE (2011)
18. Kubba, A.E., et al.: Modeling of strain energy harvesting in pneumatic tires using piezoelectric transducer. TSci. Technol. **42**(1), 16–34 (2014)

19. Lee, J., Choi, B.: Development of a piezoelectric energy harvesting system for implementing wireless sensors on the tires. Energy Convers. Manag. **78**, 32–38 (2014)
20. Aliniagerdroudbari, H., Esmaeeli, R., Hashemi, S. R., Alhadri, M., Zakri, W., Farhad, S.: A piezoelectric sandwich structure for harvesting energy from tire strain to power up intelligent tire sensors. In: 2019 IEEE Power and Energy Conference at Illinois (PECI) (pp. 1–7). IEEE (2019)
21. Yao, L., et al.: Laboratory testing of piezoelectric bridge transducers for asphalt pavement energy harvesting. Key Eng. Mat. **492**, 172–175 (2012)
22. Li C.: Road performance of common piezoelectric transducer for asphalt pavement energy harvesting. In Applied Mechanics and Materials. Trans Tech Publ. (2015)
23. Kim, H., Priya, S., Uchino, K.: Modeling of piezoelectric energy harvesting using cymbal transducers. Jpn. J. Appl. Phys. **45**(7R), 5836 (2006)
24. Yesner, G., et al.: Piezoelectric energy harvesting using a novel cymbal transducer design. In: Applications of Ferroelectrics, European Conference on Application of Polar Dielectrics, and Piezoelectric Force Microscopy Workshop (ISAF/ECAPD/PFM), 2016 Joint IEEE International Symposium on the. IEEE (2016)
25. Yesner, G., et al.: Evaluation of a novel piezoelectric bridge transducer. In: Applications of Ferroelectric (ISAF)/International Workshop on Acoustic Transduction Materials and Devices (IWATMD)/Piezoresponse Force Microscopy (PFM), 2017 Joint IEEE International Symposium on the. IEEE (2017)
26. Jasim, A., et al.: Optimized design of layered bridge transducer for piezoelectric energy harvesting from roadway. Energy **141**, 1133–1145 (2017)
27. Hazeri, S., Mulligan, C.N.: Energy harvesting by piezo-tires and their life cycle assessment. AIP Adv. **12**(6), 065112 (2022)
28. Cao, Y., et al.: Energy output of piezoelectric transducers and pavements under simulated traffic load. J. Clean. Prod. **279**, 123508 (2021)
29. Covaci, C., Gontean, A. (2020). Piezoelectric energy harvesting solutions: a review. Sens. **20**(12), 3512 (2020)
30. Jasim, A., et al.: Laboratory testing and numerical simulation of piezoelectric energy harvester for roadway applications. Appl. Energy **224**, 438–447 (2018)
31. Consortium A.: Final report including technical implementation plan (annex). Technical Research Centre of Finland (VTT), APOLLO Deliverable, **22**: p. 23 (2005)
32. Shaikh, F.K., Zeadally, S.: Energy harvesting in wireless sensor networks: a comprehensive review. Renew. Sustain. Energy Rev. **55**, 1041–1054 (2016)
33. Sekhar, M.C., et al.: A review on piezoelectric materials and their applications. Cryst. Res. Technol. **58**(2), 2200130 (2023)
34. Zhu, W., et al.: Polarization effect of road piezoelectric energy harvester under on-site road conditions. Integr. Ferroelectr. **231**(1), 185–201 (2023)
35. Cobbold, R.S.: Foundations of Biomedical Ultrasound. Oxford University Press (2006)
36. Vives A.A.: Piezoelectric transducers and applications. In: Piezoelectric transducers and applications, pp. 1–532. Springer Berlin Heidelberg
37. Makki, N., Pop-Iliev, R.: Piezoelectric power generation for sensor applications: design of a battery-less wireless tire pressure sensor. In: Smart Sensors, Actuators, and MEMS V, vol. 8066, pp. 373–382. SPIE (2011)
38. Makki, N., Pop-Iliev, R.: Battery-and wire-less tire pressure measurement systems (TPMS) sensor. Microsyst. Technol. **18**(7–8), 1201–1212 (2012)
39. Maamer, B., et al.: A review on design improvements and techniques for mechanical energy harvesting using piezoelectric and electromagnetic schemes. Energy Convers. Manag. **199**(February), 111973–111973 (2019)
40. Jain, A., et al.: Dielectric and piezoelectric properties of PVDF/PZT composites: a review. Polym. Eng. Sci. **55**(7), 1589–1616 (2015)
41. Wankhade, S.H., et al.: PVDF–PZT nanohybrid based nanogenerator for energy harvesting applications. Energy Rep. **6**, 358–364 (2020)
42. Van Den Ende, D.A., et al.: Direct strain energy harvesting in automobile tires using piezoelectric PZT-polymer composites. Smart Mater. Struct. **21**(1), 015011 (2012)
43. Sinapius, J.M.: Adaptronics-Smart Structures and Materials. Springer (2021)
44. Zhang, J., et al.: Phase morphology of nanofibre interlayers: critical factor for toughening carbon/epoxy composites. Compos. Sci. Technol. **72**(2), 256–262 (2012)
45. Magniez, K., De Lavigne, C., Fox, B.L.: The effects of molecular weight and polymorphism on the fracture and thermo-mechanical properties of a carbon-fibre composite modified by electrospun poly (vinylidene fluoride) membranes. Polymer **51**(12), 2585–2596 (2010)
46. Miclea, C., et al.: Effect of temperature on the main piezoelectric parameters of a soft PZT ceramic. Rom. J. Inf. Sci. Technol **10**(3), 243–250 (2007)
47. Makki, N., Pop-Iliev, R.: Pneumatic tire-based piezoelectric power generation. In: Active and Passive Smart Structures and Integrated Systems 2011 (2011)
48. van den Ende, D.A., Groen, W.A., van der Zwaag, S.: Robust piezoelectric composites for energy harvesting in high-strain environments. J. Intell. Mater. Syst. Struct. **24**(18), 2262–2269 (2013)
49. Song, Y., et al.: Road energy harvester designed as a macro-power source using the piezoelectric effect. Int. J. Hydrogen Energy **41**(29), 12563–12568 (2016)
50. Fu, J., et al.: Highly durable piezoelectric energy harvester based on a PVDF flexible nanocomposite filled with oriented BaTi2O5 nanorods with high power density. Nano Energy **52**, 391–401 (2018)
51. PZT Product Detail, in Alibaba. https://cnccwy.en.alibaba.com/index.html?spm=a2700.details.0.0.4fee59bcMptWmS&from=detail&productId=1600597937170 (2021)
52. Curbell Plastics. https://www.curbellplastics.com/product-category/material/pvdf/#?Shape=CRBL.SkuSheet (2021)
53. Priya, S.: Criterion for material selection in design of bulk piezoelectric energy harvesters. IEEE Trans. Ultrason. Ferroelectr. Freq. Control **57**(12), 2610–2612 (2010)
54. Bochuang Ceramic, I.N.C.: Typical values of standard piezoelectric ceramic materials. http://www.boceramic.com/products.asp?id=179 (2021)
55. Tielking, J.T., Roberts, F.L.: Tire contact pressure and its effect on pavement strain. J. Transp. Eng. **113**(1), 56–71 (1987)
56. Nega, A., Nikraz, H.: Evaluation of Tire-Pavement Contact Stress Distribution of Pavement Response and Some Effects on the Flexible Pavements. In Airfield and Highway Pavements 2017. American Society of Civil Engineers, Reston (2017)
57. Guo, M., Zhou, X.: Tire-pavement contact stress characteristics and critical slip ratio at multiple working conditions. Adv. Mater. Sci. Eng. **2019**, 1–11 (2019)
58. Bowen, C., Arafa, M.: Energy harvesting technologies for tire pressure monitoring systems. Adv. Energy Mater. **5**(7), 1401787 (2015)
59. Yesner, G., et al. Piezoelectric energy harvesting using a novel cymbal transducer design. In: 2016 Joint IEEE International Symposium on the Applications of Ferroelectrics, European Conference on Application of Polar Dielectrics, and Piezoelectric Force Microscopy Workshop (ISAF/ECAPD/PFM). IEEE, (2016)

60. Lee, J., et al.: Strain-based piezoelectric energy harvesting for wireless sensor systems in a tire. J. Intell. Mater. Syst. Struct. **26**(11), 1404–1416 (2015)
61. Roundy, S.J.: Energy Scavenging for Wireless Sensor Nodes with a Focus on Vibration to Electricity Conversion. University of California, Berkeley (2003)